Bioorganic Chemistry 114 (2021) 105127

Contents lists available at ScienceDirect

Bioorganic Chemistry

journal homepage: www.elsevier.com/locate/bioorg

Design and synthesis of novel quinazolinone-pyrazole derivatives as potential α-glucosidase inhibitors: Structure-activity relationship, molecular modeling and kinetic study

Fateme Azimi [a], Homa Azizian [b], Mohammad Najafi [c], Farshid Hassanzadeh [a], Hojjat Sadeghi-aliabadi [a], Jahan B. Ghasemi [d], Mohammad Ali Faramarzi [e], Somayeh Mojtabavi [e], Bagher Larijani [f], Lotfollah Saghaei [a,*], Mohammad Mahdavi [f,*]

[a] Department of Medicinal Chemistry, Faculty of Pharmacy and Pharmaceutical Science, Isfahan University of Medical Science, Hezar Jerib, 817416-73461 Isfahan, Iran
[b] Department of Medicinal Chemistry, School of Pharmacy-International Campus, Iran University of Medical Science, Tehran, Iran
[c] Department of Chemistry, Isfahan University of Technology, Isfahan 84156-83111, Iran
[d] School of Chemistry, University College of Science, University of Tehran, P.O. Box 14155-6455, Tehran, Iran
[e] Department of Pharmaceutical Biotechnology, Faculty of Pharmacy, Tehran University of Medical Sciences, P.O. Box 14155-6451, Tehran 1417614411, Iran
[f] Endocrinology and Metabolism Research Center, Endocrinology and Metabolism Research Institute, Tehran University of Medical Sciences, Tehran, Iran

ARTICLE INFO

Keywords:
Quinazolinone
Pyrazole
α-Glucosidase inhibitors
Enzyme inhibition
Molecular dynamic simulation

ABSTRACT

In this study, a new series of quinazolinone-pyrazole hybrids were designed, synthesized and screened for their α-glucosidase inhibitory activity. The results of the *in vitro* screening indicated that all the molecular hybrids exhibited more inhibitory activity (IC_{50} values ranging from 60.5 ± 0.3 μM-186.6 ± 20 μM) in comparison to standard acarbose (IC_{50} = 750.0 ± 10.0 μM). Limited structure–activity relationship suggested that the variation in the inhibitory activities of the compounds affected by different substitutions on phenyl rings of diphenyl pyrazole moiety. The enzyme kinetic studies of the most potent compound 9i revealed that it inhibited α-glucosidase in a competitive mode with a Ki of 56 μM. Molecular docking study was performed to predict the putative binding interaction. As expected, all pharmacophoric moieties used in the initial structure design playing a pivotal role in the interaction with the binding site of the enzyme. In addition, by performing molecular dynamic investigation and MM-GBSA calculation, we investigated the difference in structural perturbation and dynamic behavior that is observed over α-glycosidase in complex with the most active compound and acarbose relative to unbound α-glycosidase enzyme.

1. Introduction

α-Glucosidase is a membrane-bound enzyme at the epithelium of the small intestine which possesses key functions in carbohydrate digestion [1]. It catalyzes the hydrolysis of the α-1–4-glycosidic bond from the non-reducing end of carbohydrate substrates and releases absorbable glucose, which is mainly responsible for increasing blood glucose levels [2]. The control of the blood sugar level is a critical strategy in the management of diabetes mellitus, especially type II diabetes and reducing chronic complications associated with the disease. Thus, inhibition of the α-glucosidase enzyme is considered as a useful therapeutic approach for the treatment of type-2 diabetes mellitus [3,4]. Furthermore, since α-glucosidase plays a pivotal role in carbohydrate metabolism, it is considered as a therapeutic target for other carbohydrate-mediated diseases, including cancer [5], hepatitis [6] and viral infection [7,8]. Currently, carbohydrate mimics acarbose (Glucobay), miglitol (Glyset), and voglibose (Volix, Basen) are clinically approved drugs that act as inhibitors of both *α*-amylase and *α*-glucosidase enzymes [9,10]. However, continuous administration of these drugs is associated with undesirable gastrointestinal adverse reactions such as diarrhea, bloating, abdominal pain, etc. [11,12]. Based on the biological importance of α-glucosidase and the inefficiencies of existing drugs, the design and development of new α-glucosidase inhibitors are still attractive and challenging [13–18].

Pyrazole is an attractive pharmacophore in medicinal and pharmaceutical chemistry. Pyrazole and its derivatives exhibit a broad spectrum

* Corresponding authors.
E-mail addresses: saghaie@pharm.mui.ac.ir (L. Saghaei), momahdavi@tums.ac.ir (M. Mahdavi).

https://doi.org/10.1016/j.bioorg.2021.105127
Received 29 April 2021; Received in revised form 21 June 2021; Accepted 23 June 2021
Available online 29 June 2021

of pharmacological activities including anti-Alzheimer [19,20], anti-tumor [21,22], antihypertensive [23], anti-inflammatory [24,25], analgesic [26], antimicrobial [27,28], neuroprotective [29], antiviral [30], and antibacterial [31]. In particular, some of the pyrazole derivatives like Celecoxib, Viagra and Fipronil have been approved for clinical use [32]. Moreover, pyrazole scaffolds can be traced in some compounds that have been reported as potent antidiabetic and hypoglycemic agents (Fig. 1). Kenneth et al. prepared a series of pyrazole and pyrazolone derivatives as potent antihyperglycemic agents [33] and Shuangjie et al. reported the pyrazole-based derivatives as a potent glucagon receptor antagonist [34,35]. Apart from this, recent studies have shown that several entities of pyrazole act as potent α-glucosidase inhibitors. Structures of some potent pyrazole core containing α-glucosidase inhibitors are shown in Fig. 2(A–C) [36–38]. It is pertinent to mention that Teneligliptin, an oral DPP-4 inhibitor containing pyrazole, was approved for the treatment of type-II diabetes [39]. Also, report based on metabolic stability and pharmacological efficiency of pyrazole derivatives as antidiabetic agents added to our interest toward the synthesis of novel compounds containing pyrazole moiety and evaluation of their bioactivities [40,41].

On the other hand, quinazolinone and its derivatives have appealed to the medicinal chemists due to its presence in a wide range of bioactive compounds. Versatile biological properties including anti-virus [42], anti-inflammatory [43,44], anti-bacterial [45], anti-tubercular [46], anti-malaria[47], anti-cancer [48,49], anti-fungal [50], anti-allergic [51,52], anti-HIV [53] and anti-convulsant [54,55] have been successfully documented in the literature. Rudolph et al. introduced quinazolinone derivatives as orally available ghrelin receptor antagonists for the treatment of diabetes and obesity [56]. Also, recent studies have confirmed the α-glucosidase inhibitory activity of quinazolinone derivatives [57,58]. Our group has synthesized several quinazolinone-1,2,3-triazole hybrids as new *α*-glucosidase inhibitor. The results revealed that all of them presented a superior inhibitory profile than standard acarbose (IC_{50} = 181.0–474.5 μM comparing with acarbose (IC_{50} = 750.0 μM) (Fig. 2D) [59]. Peng et al. synthesized several 2-aryl quinazolinone derivatives that were subsequently assayed for α-glucosidase inhibitory activity. Among them, 2-(4-chlorophenyl)-quinazolin-4(3H)-one was identified as potent inhibitors of α-glucosidase because of its strong interaction with the enzyme (Fig. 2E) [60].

In light of the above, and also inspired by the importance of molecular hybridization for the design of new bioactive compounds, herein novel quinazolinone-pyrazole hybrids were designed and synthesized as potent α-glucosidase inhibitors. In a bid to stitch effective pharmacophores together to generate new molecules, *para*-chlorophenyl appendage on 2-position of quinazolinone moiety was maintained. Next, the pyrazole moiety insert at position 3 of quinazolinone. Amide bond was included in the design of the new hybrid as part of the initial design because of its unique features, including the polarity, amide proton exchange rate, and protein binding (Fig. 2) [61–65].

2. Result and discussion

2.1. Chemistry

The synthetic strategy for the intermediates and target compounds 9a-p has been depicted in Scheme 1. Quinazolinone 2 was obtained from the condensation of anthranilamide 1 and 4-choloro benzaldehyde in the presence of $NaHSO_3$ in DMAc. It was then alkylated with ethyl bromoacetate in acetone and under basic conditions to afforded ester 3, which was further mixed with hydrazine hydrate in methanol to form acetohydrazides 4.

The procedure for the synthesis of 1,3-disubstituted pyrazole-4-carbaldehydes 8a-p was carried out via two-step methods. Initially, condensation of different substituted acetophenones 5 with phenylhydrazine or 4-methyl phenylhydrazine in the presence of sulfuric acid in absolute ethanol afforded hydrazone intermediates 7a-p. Next, the synthesized hydrazone intermediates 8a-p undergoes Vilsmeier–Hack reaction with DMF/$POCl_3$ to form pyrazole-4-carbaldehydes derivative 8a-p. Finally, compounds 4 and variously substituted aldehyde 8a-p were refluxed overnight in ethanol in the presence of a catalytic amount of anhydrous acetic acid to get the target quinazolinone-pyrazole derivatives 9a-p.

2.2. In vitro α-glucosidase inhibitory activity

All the synthesized new hybrids 9a-p were screened for their in vitro α-glucosidase inhibition against yeast α-glucosidase in comparison to acarbose as the standard drug (Table 1). To obtain the best insight into the effects of the different substitutions on phenyl rings attached to pyrazole core, a variety of compounds 9 were synthesized. As can be

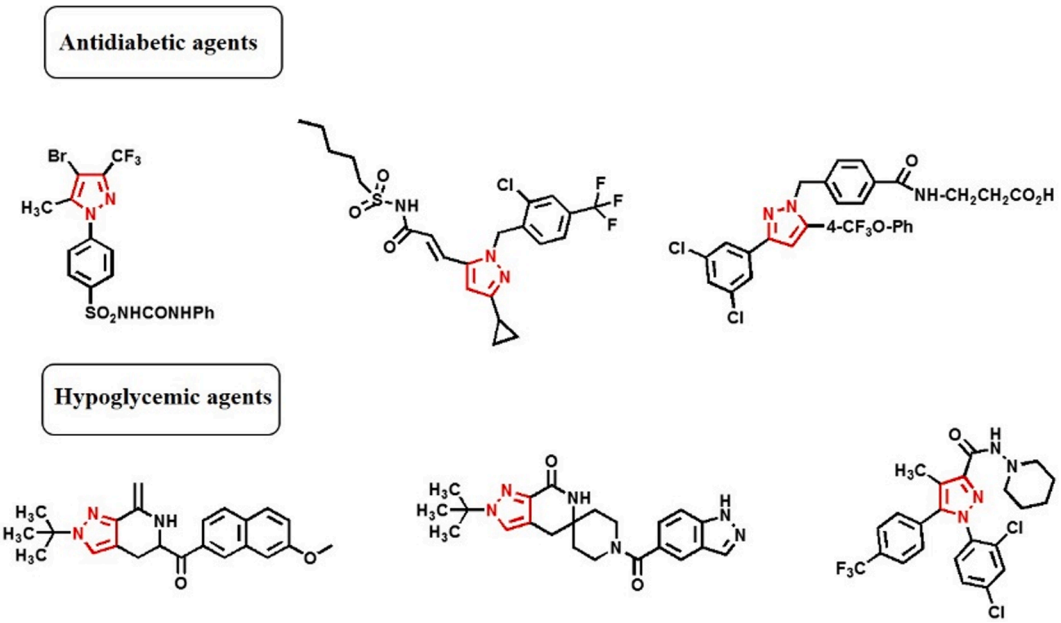

Fig. 1. Pyrazole derivatives as antidiabetic and hypoglycemic agents.

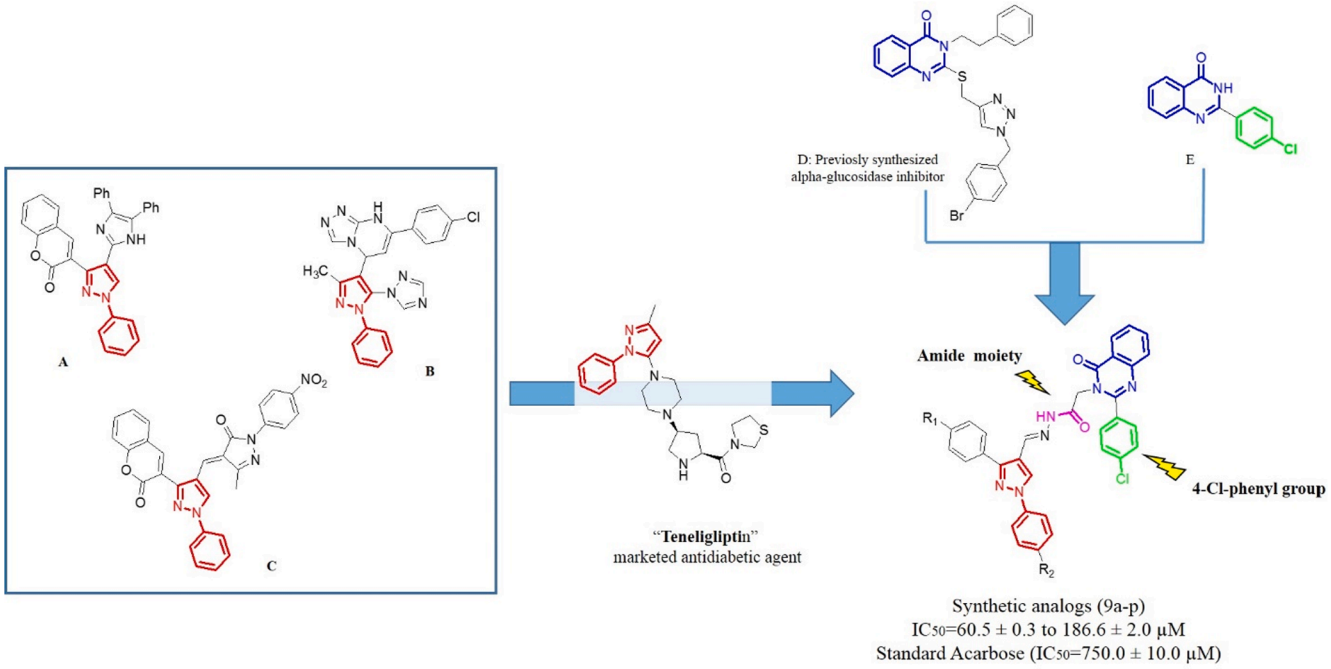

Fig. 2. Design strategy of novel quinazolinone-pyrazole derivatives as novel α-glucosidase inhibitors based on molecular hybridization of pharmacophoric units of potent reported α-glucosidase inhibitors A–D.

seen in Table 1, synthesized compounds can be considered in two categories of 9a-i (series A, Table 1, R2═H) and 9j-m (series B, Table 1, R2═CH_3) and then a limited structure–activity relationship has been also established based on variations in substitution pattern at the R_1 position. All the new synthetic derivatives displayed excellent α-glucosidase inhibitory activity having IC_{50} values in the range 60.5 ± 0.3–186.6 ± 2.0 μM and 91.7 ± 0.7–167.2 ± 1.9 μM, for 8a-i and 8j-m, respectively, when compared to standard acarbose (750 ± 10 μM). It is worth mentioning that all compounds 9 demonstrated inhibitory activities around 12–4 folds more than standard. The best activity was obtained by compound 9i having bromo group at the R_1 position and no substitution at R_2 position.

In series A, replacing bromine with other halogens (F and Cl) led to a decrease in the inhibitory activity as observed in the compounds 9g (IC_{50} = 79.5 ± 0.5 μM) and 9 h (IC_{50} = 107.1 ± 0.8 μM), respectively. It should be noted that trifluoromethyl substituted compound 9f (IC_{50} = 143.6 ± 1.6 μM) showed lower activity than other halogenated compounds. Therefore, it seems that the α-glucosidase inhibitory activity of halogenated analogous 9f-i was not only affected by the size of halogen groups but also by their electronic property of them. In this series of compounds, it was observed that the introduction of the electron-withdrawing NO_2 group (compound 9e) led to good activity with IC_{50} = 113.2 ± 1.0 μM. Finally, compounds 9b-d depicted versatile inhibitory activity affected by the electron-donating capability of the substitution. The order of activity for compounds 9b-d, was found to be 9b > 9c > 9d (IC_{50s} = 138.3, 151.7, and 176.2 μM, respectively), suggesting that an electron-donating group was less favorable to the activity.

Further investigation comes back to the series B of compounds (9j-m) which possessed a methyl group at the R_2 position. In the case of halo-substituted derivatives 9o (IC_{50} = 124.6 ± 1.1 μM) and 9p (IC_{50} = 133.6 ± 1.4 μM), comparing the corresponding inhibitory activity with their counterparts in the first category revealed that the introduction of methyl group did not induce higher activity. Compound 9k, the most active member of the series B and the third most active compound tested (IC_{50} = 91.7 ± 0.7 μM), having a methyl group at both R_1 and R_2 position. Replacement of methyl with hydroxyl or methoxy group dramatically decreased the inhibitory activity. So that compounds 9l and 9m, with IC_{50} values of 155.2 ± 1.8 and 167.2 ± 1.9 μM, respectively, showed the lowest inhibitory activity in this series of compounds. Similarly, it seems that the presence of electron-donating groups were again unfavoured for α-glucosidase inhibitory activity. In this series, NO_2 substituted derivative 9n showed the second highest activity, with an IC_{50} value of 105.7 ± 0.8 μM. It is also interesting to note that, among the synthesized compounds, derivatives with unsubstituted at R_1 position have shown less inhibitory activity, as in compounds 9a (IC_{50} = 186.6 ± 2.0 μM) and 9j (IC_{50} = 148.7 ± 1.6 μM).

From these results, it could be concluded that substitution at R_1 position as well as their electron property plays an important role in *in vitro* α-glucosidase inhibitory activity. On the other hand, the efficacy of the methyl group at the R_2 position was affected by the nature of substitutions at the R_1 position. In this regard, α-glucosidase inhibitory activity of compounds 9k, 9m, and 9n substituted with methyl, hydroxyl and nitro at the R_1 position, respectively, indicated that the introduction of methyl substituent at the R2 position improved inhibitory activity (inhibitory activity: 9k > 9b, 9m > 9d, 9n > 9e). In a different manner, the presence of methyl group at R_2 position caused bromo derivative 9p showed two-fold lower activity than its corresponding analog 8l in series A. Similarly, in chloro substituted derivative 9h, the absence of the methyl group led to better activity (inhibitory activity: 9h > 9o). Interestingly, the presence of the methyl group in methoxy derivative had a negligible effect on the inhibitory efficacity (9c and 9l).

2.3. Kinetic study

To evaluate the mechanism of inhibition of the new synthesized hybrid, the enzyme kinetic studies of the most active compound 9i were performed. The inhibition mode was determined by the Lineweaver–Burk plots and the K_i value was calculated from the second plots of the kinetic parameter (Km) versus different concentrations of inhibitor 9i (Fig. 3A–B). As can be seen in Fig. 3A, the Lineweaver–Burk plots revealed that by increasing the concentration of compound 9i, the Vmax was not affected, while the Km increased [66–69]. It indicated that compound 9i competes with the substrate for binding at the active site of the α-glucosidase enzyme. Moreover, the inhibitory constant (Ki) of this compound was calculated as 56 μM.

Similarly, many recently developed organic-nitrogen compounds

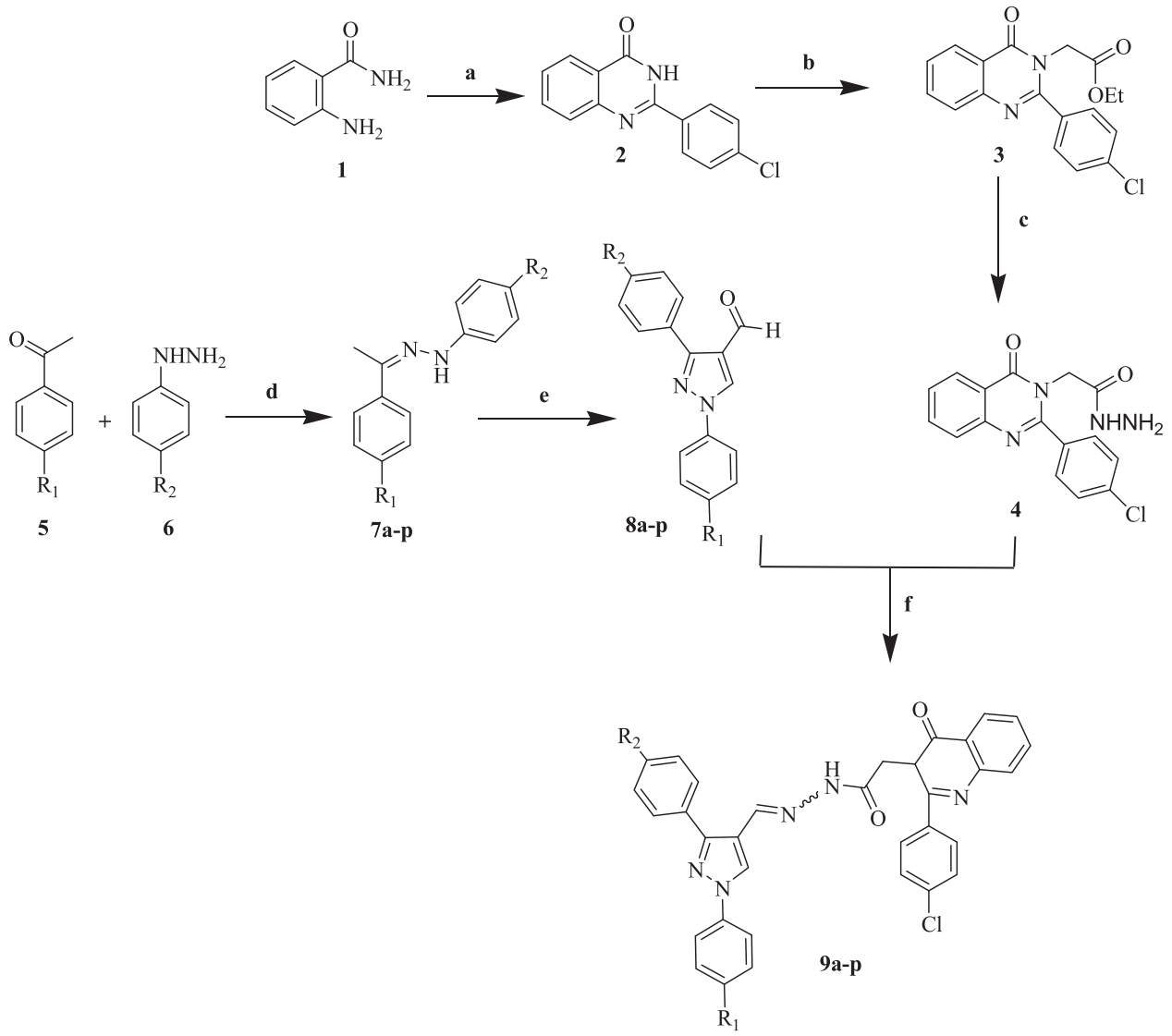

Scheme 1. Synthesis of target compounds 10a-p. Reagents and conditions: (a) $NaHSO_3$, DMAC, 180 °C, 12 h; (b) Ethyl bromoacetate, K_2CO_3, acetone, rt, overnight; (c) $N_2H_4{\cdot}H_2O$, EtOH, reflux, 4 h; (d) H_2SO_4, EtOH, reflux, 8–12 h; (e) DMF, $POCl_3$, 60 °C, 5–8 h; (f) AcOH, EtOH, reflux, overnight.

competitively inhibited the α-glucosidase [70,71]. Interestingly, to the best of our knowledge, none of the reported pyrazole-based inhibitor competitively inhibited the enzyme activity.

2.4. α-Amylase inhibition assay

Inhibition of α-amylase is also a relevant strategy to control post-prandial hyperglycemia through delayed carbohydrate digestion [72]. In this regard, the most potent compounds (9i, 9g, and 9k) were also evaluated for their inhibitory potential against α-amylase. Results revealed that these compound had no activity against α-amylase (at 300 μM) when compared with acarbose as a standard α-amylase inhibitor ($IC_{50} = 108 \pm 0.71$ μM).

Non-halogenated derivative in recent developed bis-azo-containing Schiff base exhibited the highest inhibitory potential against both enzymes (α-glucoside and α-amylase) [70].

2.5. Docking

To acquire insight into the binding interactions of the newly synthesized quinazolinone-pyrazole derivatives in the active site of α-glucosidase, in silico docking studies were carried out by employing the GOLD 5.3 tool. Since the x-ray crystallographic structure *S. cerevisiae* α-glucosidase is still not available, a homology model of this enzyme was built and validated according to our reported method [73]. Compounds 9i, 9g, 9k, 9m, and 9a were selected for docking studies. The superposed structure of these compounds and details of their interactions in the active site of a-glucosidase is shown in Fig. 4.

From the docking calculation study, it was observed that compounds well nested into the active pocket of α-glucosidase and several favorable interactions support the high potency against the enzyme. The predicted binding mode of studied compounds indicated that the following interactions were mutual for them. (1) pyrazole core made *T*-shaped π-stacking interaction with Phe177, whereas the phenyl groups attached to the pyrazole moiety established hydrophobic interaction with residues Arg439, Tyr71, Ala278 and Phe157. (2) π-alkyl and π-π *T*-shaped interactions formed between quinazolinone moiety and Arg312 and Phe157, respectively. (3) Furthermore, 4-chlorophenyl group directing toward the hydrophobic pocket comprising Phe300 and Val303. This pharmacophore showed two interactions with Phe300 and Val 303 through chloro and one π-alkyl interaction with Val303 through phenyl ring, which could further fitted ligands tightly into the active site of the enzyme. (4) The amide linker forms two hydrogen bonds with active site residues, which played a significant role in stabilizing the enzyme-

Table 1
In vitro α-glucosidase inhibitory activity of compounds 9a-p.

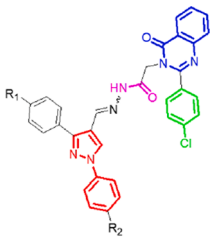

9a-p

Compound	R_1	R_2	IC_{50}(μM)[a]
9a	H	H	186.6 ± 2.0
9b	CH_3	H	138.3 ± 1.5
9c	OCH_3	H	151.7 ± 1.8
9d	OH	H	176.2 ± 1.9
9e	NO_2	H	113.2 ± 1.0
9f	CF_3	H	143.6 ± 1.6
9g	F	H	79.5 ± 0.5
9 h	Cl	H	107.1 ± 0.8
9i	Br	H	60.5 ± 0.3
9j	H	CH_3	148.7 ± 1.6
9k	CH_3	CH_3	91.7 ± 0.7
9l	OCH_3	CH_3	155.2 ± 1.8
9m	OH	CH_3	167.2 ± 1.9
9n	NO_2	CH_3	105.7 ± 0.8
9o	Cl	CH_3	124.6 ± 1.1
9p	Br	CH_3	133.6 ± 1.4
Acarbose	–	–	750.0 ± 10.0

[a] Values are the mean ± SD. All experiments were performed at least three times.

inhibitor complex. Asp408 made H-acceptor interaction with NH unit of amide moiety while Tyr313 formed H-acceptor interaction with the carbonyl of the same moiety. Similar types of interactions were also observed in newly developed *N*-alkyl–deoxynojirimycin derivatives [71].

Therefore, as expected, all pharmacophores used in the design of new hybrid have participated in binding with the catalytic residue that play a significant role in enhancing inhibition activity against the α-glucosidase enzyme.

The most potent compound 9i made further interactions in addition to those described above and hydrophobic interactions have a greater contribution for binding of it (Fig. 4B). Bromo substituted phenyl is positioned in a hydrophobic pocket comprising the side chains of Asp68, His348, Tyr71 and Arg439 that allows the formation of highly stable complexes. As can be seen in the Fig. 5B and C, the comparison of interaction modes of compound 9g and 9i revealed that diphenyl pyrazole moiety in compound 9g, unlike compound 9i established fewer hydrophobic interactions with the active site residues. On the other hand, the oxygen carbonyl of amide moiety of the compound 9g formed additional hydrogen bond interaction with Arg439, which could be a key factor in stabilizing this compound in the active site of the enzyme. Compound 9k, the most active compound in series B, formed two additional hydrogen bonds compared to compound 9i. Arg439 established a hydrogen bond with the oxygen atom of amide carbonyl and Tyr313 formed a hydrogen bond with carbonyl group of quinazolinone moiety. Also, this compound is involved in hydrophobic interactions with several residues such as His348, His245, His279, Tyr71 and Ala278 through methyl-substituents at R_1 and R_2 (Fig. 4D). For further investigation, the interaction mode of least active compounds in the series A and B (9a and 9m) were also analyzed in detail. Similar to compound 9g, an additional hydrogen bond is established between the oxygen atom of the amide carbonyl of compound 9a and the side chains of Arg439 (Fig. 4E). Compound 9m showed additional hydrophobic interactions with His245, Leu218, Ala278 and Phe157 through methyl-substituted phenyl group while hydroxyl substitution was making a hydrogen bond with the oxygen atom of Asp68 (Fig. 4F). Other interactions are the same in both compound 9a and 9m.

Further studies on gold fitness docking scores of compounds 9i (72.09), 9g (74.46), 9k (969.67), 9a (77.27) and 9m (64.48) revealed that they bound more easily to the active site than the standard drug acarbose (35.71). However, there was no good correlation between the docking scores and biological activities of compounds, indicating that some other factors rather than their binding mode to the active site were important.

2.6. Molecular dynamic (MD) simulation

MD simulation was performed in order to understand the effect of the best biologic active compound over the enzyme active site [74]. For this purpose, the structural perturbations incurred by the most potent compound (9i) has been investigated through the study the RMSD, RMSF and their effect on the active site environment in comparison to acarbose as α-glycosidase standard inhibitor and the apo-enzyme. The appropriate pose for MD simulation procedure of the compound 9i and acarbose were achieved by induced fit docking method.

The stability of protein–ligand complex trajectories assessed by

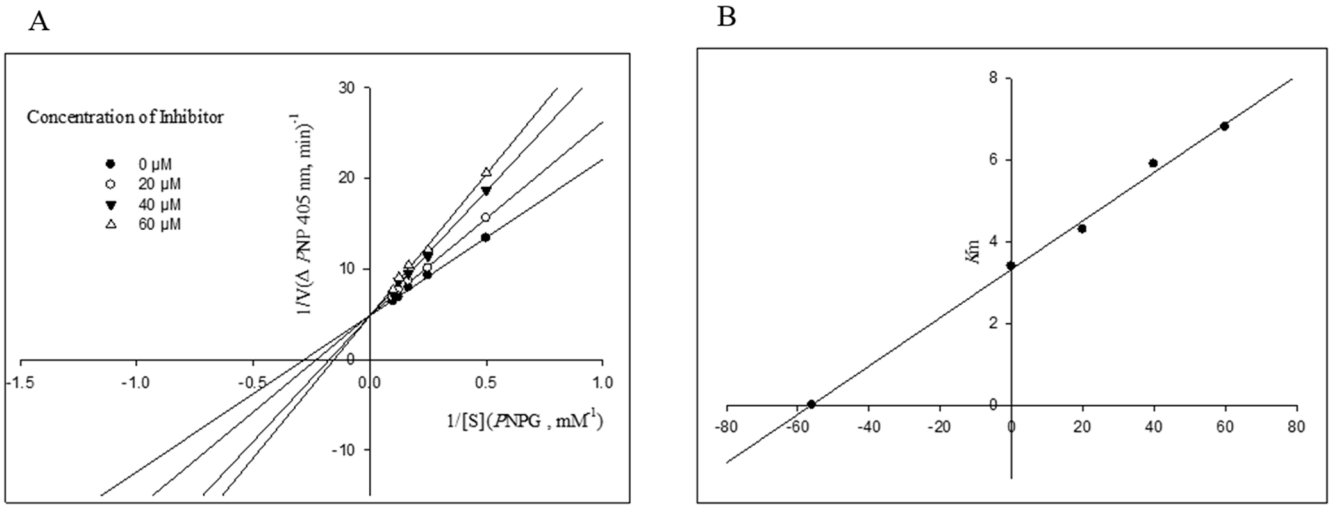

Fig. 3. Kinetic study of α-glucosidase inhibition by compound 9i. (A) The Lineweaver–Burk plot in the absence and presence of different concentrations of compound 9i (μM); (B) the secondary plot between 1/Vmax and various concentrations of compound 9i.

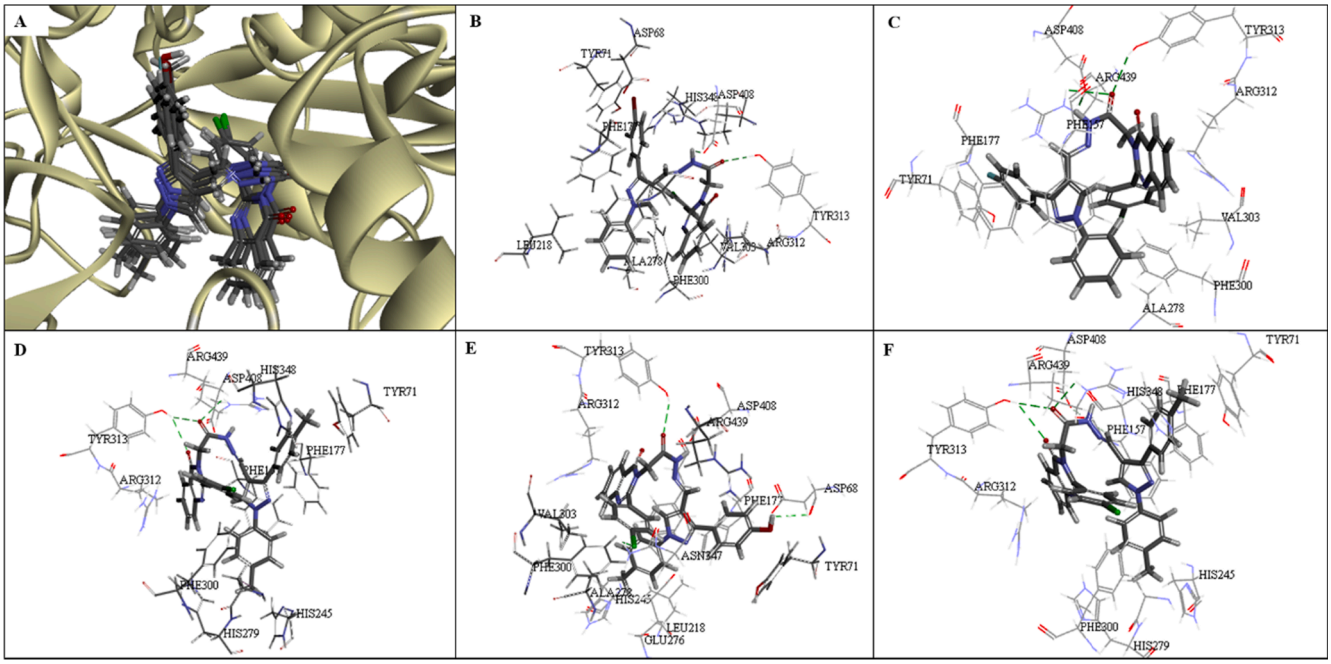

Fig. 4. (a) 9i, 9g, 9k, 9m and 9a superimposed in the active site pocket of modeled α-glucosidase. The predicted binding modes of (B) 9i, (C) compound 9g, (D) compound 9k (E) compound 9m and (F) compound 9a, in the active site pocket. Residues that may be involved in the interactions of compound binding are drawn with stick model and shown in different colors. (The colored symbols are as following, dark gray: carbon, light gray: hydrogen, red: oxygen, blue: nitrogen, green: chlorine. The possible hydrogen-bond interactions are indicated with dashed green lines). (For interpretation of the references to color in this figure legend, the reader is referred to the web version of this article.)

analyzing the root mean square deviation (RMSD) of the enzymes's backbone over the 20 ns MD simulation. The RMSD value of the unbounded α-glycosidase enzyme depicts higher RMSD value than the other two bounded-state enzyme complexes. The RMSD value significantly increased during the first 5 ns up to 2.7 Å and steadily fluctuated to the next 10 ns and become more stable for the last 5 ns of simulation time with the value of 2.6 Å. Moreover, based on the RMSD value of α-glycosidase complexed with acarbose and compound 9i, the bounded state enzymes were stable during the simulation time with the lower RMSD value of 1.8 Å and 2 Å, respectively (Fig. 5). The mentioned outcome may cause as a result of more structural rigidity due to the active site bounding state and proposed the importance of active site domain on the structural flexibility of α-glycosidase enzyme.

The RMSD value for the 5 ns at the terminal section of MD simulation was used to investigate the structural specificity of α-glycosidase-ligand complexes.

Moreover, the detailed residue-based flexibility of protein structure

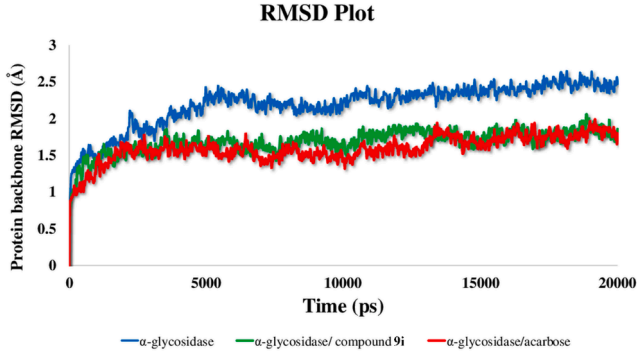

Fig. 5. RMSD of the α-glycosidase backbone in complexed with acarbose (in red), compound 9i (in green) and the unbound enzyme (in blue) for over 20 ns MD simulation time. (For interpretation of the references to color in this figure legend, the reader is referred to the web version of this article.)

can be evaluated through investigating the RMSF value in which evaluate the fluctuation of the protein backbone structure from its average position throughout the whole simulation time [75]. The residue RMSF values of the α-glycosidase unbounded enzyme and the enzyme in the bounded state showed that, the unbounded enzyme (blue color line) had higher RMSF fluctuations compared to the α-glycosidase bound-states (green and red colored line) (Fig. 6-a). According to the result, the mentioned lower RMSF value occurs upon ligand binding to the enzyme, in which residues movement decrease as a result of non-bonding interaction between the ligand and the enzyme active site residues. Moreover, Fig. 6a depicted that there are four structural segments which revealed different RMSF pattern upon ligand binding including; B domain loop and the active site lid (both in pink dash box), A domain and B domain sides of the active site entrance (orange and blue dash boxes, respectively).

Based on Fig. 6a and b, the RMSF value of the B domain loop residues would have decreased in α-glycosidase/acarbose and compound 9i bound-state rather than unbounded α-glycosidase enzyme. Furthermore, both acarbose and compound 9i bonding state show the same RMSF value and the ligand-binding pattern except the region over the active site lid. The flexibility of the active site lid was not only the lowest in unbounded enzyme, but the mentioned segment flexibility revealed higher in α-glycosidase complexed with acarbose rather than compound 9i. Furthermore, Fig. 6b depicts the interaction of acarbose and compound 9i with several residues located both on A and B domain sides of the active site mouth. Also, acarbose showed more interaction with the A side domain of the active site entrance (orange dash line in α-glycosidase/acarbose), while compound 9i provided a higher number of interactions with the residues of the B domain side (blue dash line in α-glycosidase/compound 9i). So, it can be proposed that the lower RMSF value of the active site lid has occurred as a result of higher ligand interactions with the B domain side of the active site mouth. In addition, Fig. 6c and d depict the close-up representation of the active site mouth in association with the corresponding residues of A and B domains at both sides of the active site entrance.

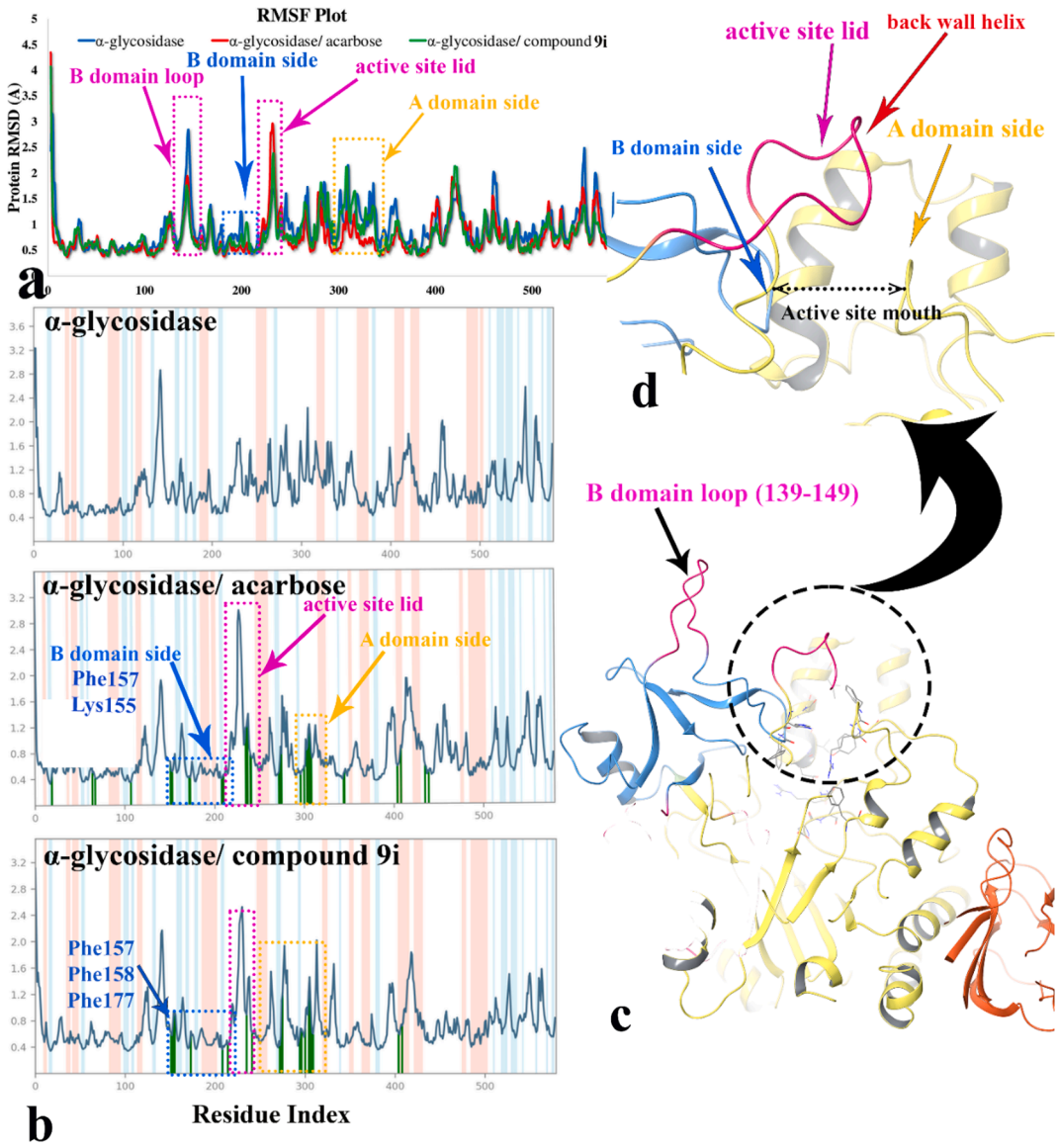

Fig. 6. RMSF plot of the α-glycosidase backbone in complexed with compound 9i (in yellow) and acarbose (in green) and the unbounded enzyme (in red) for over 20 ns MD simulation time (a). Ligand binding location of α-glycosidase in bound and unbound-state for over 20 ns MD simulation time (α-helical and ß-strand regions are highlighted in red and blue backgrounds, respectively) (b). 3D representation of α-glycosidase structure. Enzyme domain of A, B and C are colored in yellow, blue, and orange, respectively. The the flexible regions correspond to the B domain loop and the active site lid are colored in pink (c). Close-up representation of α-glycosidase active site (d). (For interpretation of the references to color in this figure legend, the reader is referred to the web version of this article.)

Overall, based on the result of the RMSF plot, acarbose and compound 9i have almost the same interaction pattern through the whole α-glycosidase active site structure. The only dissimilarity comes from the active site lid flexibility in which we can propose that compound 9i along with more interaction over the B domain side of the active site entrance, has a dominant effect in the rigidity of active site lid rather than acarbose which has more interaction with the A domain side of the α-glycosidase active site entrance.

Fig. 7a and b represent the detailed orientation and interactions that occurred more than 30% of the simulation time during the equilibrated phase over the α-glycosidase complexed with compound 9i. The interaction inspection depicts compound 9i stabilized into the enzyme domains by interacting with residues Phe300, Glu276, Arg212, Arg312, Pro309, and Leu218 from the A domain side and Phe157 and Phe177 from the B domain side of the active site mouth. In the case of acarbose, it disposed vertically and formed non-binding interactions with residues Phe311, Asn241, Arg439, Asp68, His245, Asp349, Asp214, which belong to the domain A of the enzyme (Fig. 7c). Furthermore, Fig. 7a and b represent four important structural moieties in stabilizing compound 9i into the active site of α-glycosidase. The first one is the phenyl pyrazole and the quinazoline rings, which oriented toward the front side of the active site and interacted with Phe177 and Phe157 at the B side of the active site mouth through Van Der Waals and *T*-shape π-π hydrophobic interactions for about 51% and 60% of the simulation time, respectively. The next part is related to the bromo phenyl and chloro phenyl moieties which pointed toward the back part of the active site and mainly interacted with Arg212 and Arg312 residues through π-cation interactions for almost the whole amount of simulation time (95% and 91% of MD time, respectively). Along with these interactions, the acetohydrazide group interacted with Asp408 located at the back part of the active site (previously known as back wall helix) through H-bond interaction with the C═O group for about 61% of the simulation time. Besides these stabilizing interactions, the pyrazole ring provided steady interaction with Glu276 which is one of the active site catalytic residue for significantly 85% of simulation time.

Based on the MD study, it can reveal that compound 9i not only like

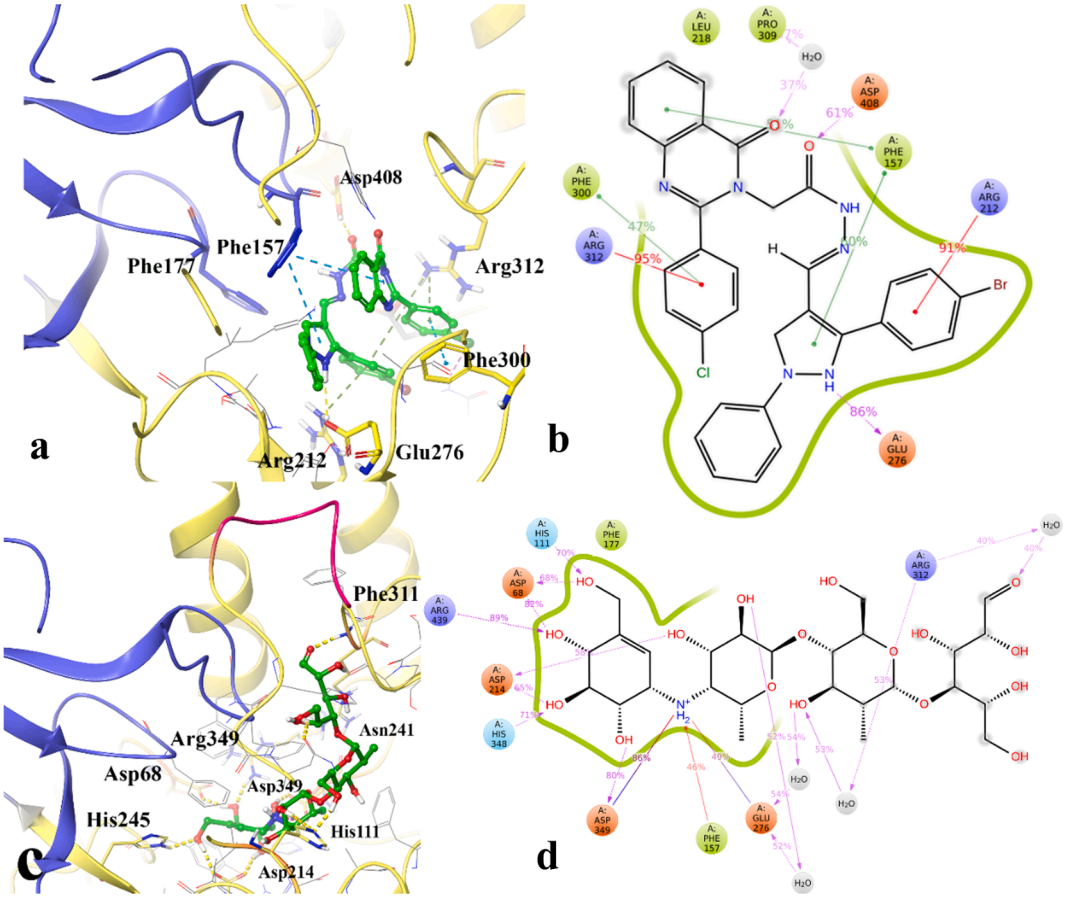

Fig. 7. The detailed orientation and ligand atom interactions that occurred more than 30.0% of the simulation time during the equilibrated phase over α-glycosidase complexed with compound 9i (a, b) and acarbose (c, d). Domain A, domain B and the flap region covered the mouth of the active site colored in yellow, blue and pink, respectively. (For interpretation of the references to color in this figure legend, the reader is referred to the web version of this article.)

as acarbose stabilized through hydrophobic and H-bond interaction with A domain side of the active side mouth (Fig. 7d) but also provided persistent and strong interactions with the B domain side of the active side mouth, the back side of the active site and the catalytic residue during the MD simulation time which may propose the contribution to the higher α-glycosidase inhibition activity of the mentioned compound.

Finally, the binding free energies calculated by performing the MM-GBSA method, is which known as one of the rigorous and efficient methods to estimate relative binding affinities have been performed to predict the strength of compound's affinity over the enzyme active site [76,77]. In this way, a number of 102 snapshots were extracted at time interval of 50 ps from the last 5 ns of equilibrated MD trajectories which can provide scope for predicting the biological activity of compound 9i. The calculated binding free energies (ΔG_{bind}) and the individual energy components reveal that the binding free energies of α-glycosidase complexed with compound 9i are obviously higher than acarbose (-93.14 ± 7.80 vs. -62.49 ± 2.90 kcal.mol^{-1}, respectively) during the equilibrated phase of MD simulation time which may attribute to the more stabilizing effect of compound 9i over the A and B domain of the enzyme.

3. Conclusion

In conclusion, a novel series of quinazolinone-pyrazole derivatives were designed, synthesized and evaluated for α-glucosidase inhibitory activities. The results of the in vitro screening indicated that newly synthesized hybrids demonstrated inhibitory activities around 12–4 folds more than acarbose as standard drug. Among them, compound 9i with the IC_{50} values of 60.5 ± 0.3 μM was found to be the most potent compound. The analysis of the structure–activity relationship indicated that substitution at R_1 position as well as their electron property plays an important role in *in vitro* α-glucosidase inhibitory activity. On the other hand, the efficacy of the methyl group at the R_2 position was affected by the nature of substitutions at the R_1 position. Analysis of the kinetics of enzyme inhibition indicated that compound 9i inhibited α-glucosidase in a competitive inhibition manner (Ki = 56 μM). Further, the in silico studies were performed to get insights into the molecular interaction of compounds with the active site of the enzyme. Docking study of compounds 9i, 9g, 9k, 9m and 9a revealed that they behave almost similar to exhibit the inhibitory potential and well fitted in the active site of α-glucosidase through both hydrophobic and hydrogen interactions. As expected, all pharmacophoric moiety used in the initial structure design (biphenyl pyrazole, 2-(4-chlorophenyl)-quinazolin-4(3H)-one and amide moiety) playing a pivotal role in the interaction with the binding site of the α-glucosidase enzyme. Hence, these compounds could be promising hits for further research towards the treatment of hyperglycemia and associated disorders. MD simulations showed compound 9i oriented inside the active site and stabilized through four important structural moieties; the phenyl pyrazole and the quinazoline rings which oriented toward the front side of the active site, the bromo phenyl and the chloro phenyl moiety which pointed toward the back part of the active site, the acetohydrazide group interacted at the back part of the active site and the pyrazole ring provided steady interaction with Glu276 which is one of the active site catalytic residue. These groups constructed a new nucleus which provided a significant role for inhibition activity of the mentioned compound.

4. Experimental

All the chemicals and solvents were purchased from Merck (Germany) and Sigma Aldrich (USA). Melting points (mp) of all derivatives were measured on a Kofler hot stage apparatus and uncorrected. Reactions were monitored by thin-layer chromatography (TLC) using precoated silica-gel plates (Merck, TLC silica gel 60 F254), and the plots were visualized through UV light at wavelengths of 254 and 365 nm. ^{1}H and ^{13}C NMR spectra was recorded on Avance Bruker AV-500 MHz spectrometer in DMSO-d_6 and tetramethylsilane was used as internal standard. Infrared spectra (IR) were recorded on Shimadzu 8400 S FT-IR using KBr disc. Elemental analysis of title compounds 9a-p was performed on an Elemental Analyzer system GmbH VarioEL CHN mode.

4.1. General procedure for the synthesis of 2-(4-chlorophenyl)quinazolin-4(3H)-one 2

Anthranilamide 1 (20 mmol) was treated with 4-choloro benzaldehyde (20 mmol) in DMAC in the presence of $NaHSO_3$ (40 mmol) and the mixture was heated at 180 °C for 15 h. After completion of the reaction (checked by TLC), the mixture was cooled to room temperature and poured into ice–water (100 mL). The formed precipitate was collected by filtration and washed successively with water. The product was recrystallized from ethyl acetate/petroleum ether to provide 2-(4-chlorophenyl)quinazolin-4(3H)-one 2 as pale yellow solid [60].

4.2. General procedure for the synthesis of ethyl 2-(2-(4-chlorophenyl)-4-oxoquinazolin-3(4H)-yl)acetate 3

The mixture of 2-(4-chlorophenyl)quinazolin-4(3H)-one 2 (15 mmol) and Anhydrous K_2CO_3 (30 mmol) in acetone (15 mL) stirred for 10 min at room temperature. Then, ethyl bromoacetate (15 mmol) was added to the stirring solution and the reaction was continued at room temperature for 15 h. Upon completion, checked by TLC, the mixture was poured into 100 mL of water. The precipitated products 3 were filtered off, washed with water, and recrystallized from ethanol–water [78].

4.3. General procedure for the synthesis of 2-(2-(4-chlorophenyl)-4-oxoquinazolin-3(4H)-yl)acetohydrazide 4

5 mL hydrazine hydrate was added to a solution of compound 3 (10 mmol) in ethanol (15 mL). The reaction mixture was heated under reflux for 6 h. Reaction progress was monitored using TLC. After completion of the reaction, the solvent volume was reduced to half the original volume in a rotary evaporator, under reduced pressure. Upon cooling, the separated solid was filtered, washed with water and dried. The solid obtained was recrystallized with ethanol to get crystals of pure product 4 [78].

4.4. General procedure for the synthesis of 1,3-disubstituted pyrazole-4-carbaldehydes 8a-p

A mixture of substituted acetophenone 6 (10 mmol) and 4-substituted phenylhydrazine 7 (12 mmol) in ethanol (15 mL) was heated under reflux in the presence of a catalytic amount of anhydrous acetic acid (0.5 mL) at 70 °C for 8–12 h. After completion of the reaction, the mixture was cooled at room temperature and the precipitate was allowed to settle down, filtered, washed with ethanol and dried in vacuo to afford hydrazone intermediate 7a-p. In the next step, hydrazone intermediate 7a-p (10 mmol) was added to a cold solution of dimethylformamide (10 mL) and phosphoryl chloride (30 mmol) and the resulting mixture was heated at 60 °C for 5–8 h. After the completion of the reaction (checked by TLC), the mixture was cooled and poured into a slurry of ice/saturated solution of sodium bicarbonate. The solid product obtained was filtered, washed with and crystallized in ethanol to afford pure product [79].

4.5. General procedure for the synthesis of quinazolinone-pyrazole hybrids 9a-p

Equimolar quantities (1 mmol) of appropriate pyrazole-4-carbaldehyde derivative 8a-p and 2-(2-(4-chlorophenyl)-4-oxoquinazolin-3(4H)-yl)acetohydrazide 4 were dissolved in warm ethanol with a catalytic amount of glacial acetic acid and the reaction was refluxed for>16 h. After completion (TLC), the solvent was evaporated in vacuum to half its volume and cooled to room temperature. After cooling, the solid obtained was separated by filtration, washed with water, dried, and recrystallized with ethanol to get the target compound 9a-p. The target compounds were obtained as a mixture of Z and E isomers. The percentage of isomers was calculated by NMR [80].

4.5.1. 2-(2-(4-Chlorophenyl)-4-oxoquinazolin-3(4H)-yl)-N′-((1,3-diphenyl-1H-pyrazol-4-yl)methylene)acetohydrazide (9a)

White powder; yield: 83%, mp 248–249 °C. IR (KBr, cm^{-1}): 3450 (N—H), 3053 (C—H), 1668 (C═O), 1649 (C═O), 1639 (C═N). ^{1}H NMR (400 MHz, DMSO-d_6, mixture of two isomers E:Z = 58%:42%) δ 11.83 (s, 1H, NH), 11.61 (s, 1H, NH), 9.11 (s, 1H, H_5-pyr), 8.99 (s, 1H, H_5-pyr), [8.53–8.38 (m, 2H), 8.30–8.24 (m, 2H), 8.06–7.94 (m, 4H), 7.82–7.67 (m, 3H), 7.60–7.41 (m, 7H), 7.40–7.32 (m, 1H)] (19H, Ar—H and CH═N), 5.67 (s, 2H, CH_2), 5.25 (s, 2H, CH_2). ^{13}C NMR (101 MHz, DMSO, mixture of two isomers) δ 167.8, 165.9, 165.7, 163.2, 157.5, 151.8, 151.2, 140.7, 138.9, 137.0, 135.9, 135.8, 135.7, 135.6, 134.6, 132.2, 131.9, 129.7, 129.6, 129.5, 129.5, 128.7, 128.6, 128.6, 128.5, 128.5, 128.4, 128.4, 128.3, 127.6, 127.5, 127.1, 126.9, 123.5, 123.3, 118.7, 118.6, 116.7, 116.5, 114.3, 114.3, 64.6, 63.5. Anal. Calcd for $C_{32}H_{23}ClN_6O_2$: C, 68.75; H, 4.15; N, 15.03. Found: C, 68.02; H, 4.56; N, 15.66.

4.5.2. 2-(2-(4-Chlorophenyl)-4-oxoquinazolin-3(4H)-yl)-N′-((1-phenyl-3-p-tolyl-1H-pyrazol-4-yl)methylene)acetohydrazide (9b)

White powder; yield: 85%, mp 259–261 °C. IR (KBr, cm^{-1}): 3405 (N—H), 3120 (C—H), 1689 (C═O), 1655 (C═O), 1644 (C═N). ^{1}H NMR (400 MHz, DMSO-d_6, mixture of two isomers E:Z = 58%:42%) δ 11.82 (s, 1H, NH), 11.60 (s, 1H, NH), 9.09 (s, 1H, H_5-pyr), 8.96 (s, 1H, H_5-pyr), [8.52–8.40 (m, 2H), 8.31–8.20 (m, 2H), 8.05–7.95 (m, 4H), 7.76–7.59 (m, 3H), 7.58–7.46 (m, 4H), 7.42–7.30 (m, 3H)] (18H, Ar—H and CH═N), 5.70 (s, 2H, CH_2), 5.25 (s, 2H, CH_2), 2.40 (s, 3H, CH_3), 2.33 (s, 3H, CH_3). ^{13}C NMR (101 MHz, DMSO, mixture of two isomers) δ 167.8, 166.0, 163.1, 157.5, 151.8, 151.2, 151.2, 140.8, 138.9, 138.1, 138.0, 137.1, 135.9, 135.6, 134.6, 129.7, 129.6, 129.5, 129.5, 129.3, 129.3, 129.1, 129.0, 128.6, 128.2, 128.1, 127.6, 127.5, 127.1, 126.8, 123.5, 123.3, 118.7, 118.6, 116.6, 116.4, 114.3, 114.3, 64.6, 63.5, 20.8, 20.8. Anal. Calcd for $C_{33}H_{25}ClN_6O_2$: C, 69.17; H, 4.40; N, 14.67. Found: C, 69.56; H, 3.88; N, 14.98.

4.5.3. 2-(2-(4-Chlorophenyl)-4-oxoquinazolin-3(4H)-yl)-N′-((3-(4-methoxyphenyl)-1-phenyl-1H-pyrazol-4-yl)methylene)acetohydrazide (9c)

White powder; yield: 79%, mp 241–243 °C. IR (KBr, cm^{-1}): 3450 (N—H), 3115 (C—H), 1678 (C═O), 1649 (C═O), 1639 (C═N). ^{1}H NMR (400 MHz, DMSO-d_6, mixture of two isomers E:Z = 58%:42%) δ 11.82 (s, 1H, NH), 11.60 (s, 1H, NH), 9.07 (s, 1H, H_5-pyr), 8.96 (s, 1H, H_5-pyr), [8.51–8.42 (m, 2H), 8.34–8.18 (m, 2H), 8.03–7.98 (m, 4H), 7.74–7.67 (m, 3H), 7.57–7.50 (m, 4H), 7.43–7.27 (m, 1H), 7.12–7.06 (m, 2H)] (18H, Ar—H and CH═N), 5.70 (s, 2H, CH_2), 5.25 (s, 2H, CH_2), 3.84 (s, 3H, OCH_3), 3.76 (s, 3H, OCH_3). ^{13}C NMR (101 MHz, DMSO, mixture of two isomers) δ 167.8, 166.0, 165.7, 163.1, 159.5, 159.4, 157.5, 151.6, 151.2, 151.0, 140.9, 138.9, 137.2, 135.9, 135.8, 135.7, 135.6, 134.6, 129.7, 129.7, 129.7, 129.6, 129.5, 129.5, 128.6, 128.2, 127.6, 127.5, 127.1, 126.8, 124.5, 124.2, 123.5, 123.3, 118.6, 118.5, 116.5, 116.2, 114.3, 114.3, 114.1, 113.9, 63.5, 55.2, 55.1. Anal. Calcd for $C_{33}H_{25}ClN_6O_3$: C, 67.29; H, 4.28; N, 14.27. Found: C, 67.62; H, 3.88; N,

14.82.

4.5.4. 2-(2-(4-Chlorophenyl)-4-oxoquinazolin-3(4H)-yl)-N′-((3-(4-hydroxyphenyl)-1-phenyl-1H-pyrazol-4-yl)methylene)acetohydrazide (9d)

White powder; yield: 81%, mp 256–258 °C. IR (KBr, cm^{-1}): 3477 (N—H), 3035 (C—H), 1681 (C═O), 1651 (C═O), 1642 (C═N). ^{1}H NMR (400 MHz, DMSO-d_6, mixture of two isomers E:Z = 58%:42%) δ 11.91 (s, 1H, NH), 11.68 (s, 1H, NH), 9.15 (s, 1H, H_5-pyr), 9.03 (s, 1H, H_5-pyr), [(8.63–8.49 (m, 2H), 8.43–8.29 (m, 2H), 8.13–8.07 (m, 4H), 7.85–7.81 (m, 1H), 7.74–7.58 (m, 6H), 7.49–7.43 (m, 1H), 7.05–6.99 (m, 2H)] (18H, Ar—H and CH═N), 5.82 (s, 2H, CH_2), 5.36 (s, 2H, CH_2). ^{13}C NMR (101 MHz, DMSO, mixture of two isomers) δ 167.8, 166.0, 165.7, 163.1, 157.9, 157.8, 157.5, 152.1, 151.4, 151.2, 141.0, 139.0, 137.4, 135.9, 135.9, 135.7, 135.6, 134.6, 129.7, 129.7, 129.7, 129.6, 129.5, 129.5, 128.6, 128.5, 128.0, 127.6, 127.5, 126.8, 126.7, 123.5, 123.3, 122.8, 122.6, 118.6, 118.4, 116.3, 116.1, 115.5, 115.3, 114.3, 64.6, 63.5. Anal. Calcd for $C_{32}H_{23}ClN_6O_3$: C, 66.84; H, 4.03; N, 14.62. Found: C, 66.23; H, 4.35; N, 14.24.

4.5.5. 2-(2-(4-Chlorophenyl)-4-oxoquinazolin-3(4H)-yl)-N′-((3-(4-nitrophenyl)-1-phenyl-1H-pyrazol-4-yl)methylene)acetohydrazide (9e)

White powder; yield: 85%, mp 268–270 °C. IR (KBr, cm^{-1}): 3448 (N—H), 3045 (C—H), 1680(C═O), 1654 (C═O), 1640 (C═N). ^{1}H NMR (400 MHz, DMSO-d_6, mixture of two isomers E:Z = 57%:43%) δ 11.96 (s, 1H, NH), 11.70 (s, 1H, NH), 9.17 (s, 1H, H_5-pyr), 9.06 (s, 1H, H_5-pyr), [8.50–8.48 (m, 1H), 8.42–8.22 (m, 5H), 8.17–8.10 (m, 2H), 8.05–7.96 (m, 4H), 7.75–7.70 (m, 1H), 7.62–7.49 (m, 4H), 7.44–7.38 (m, 1H)] (18H, Ar—H and CH═N), 5.61 (s, 2H, CH_2), 5.28 (s, 2H, CH_2). ^{13}C NMR (101 MHz, DMSO, mixture of two isomers) δ 167.9, 165.9, 157.5, 151.2, 148.6, 147.0, 138.8, 138.7, 136.5, 135.9, 135.6, 134.6, 130.0, 129.7, 129.6, 129.5, 129.5, 129.4, 128.9, 128.6, 127.6, 127.5, 127.3, 123.7, 123.6, 123.3, 118.9, 118.8, 117.4, 114.3, 64.5, 63.4. Anal. Calcd for $C_{32}H_{22}ClN_7O_4$: C, 63.63; H, 3.67; N, 16.23. Found: C, 63.25; H, 3.12; N, 16.45.

4.5.6. 2-(2-(4-Chlorophenyl)-4-oxoquinazolin-3(4H)-yl)-N′-((1-phenyl-3-(4(trifluoromethyl)phenyl)-1H-pyrazol-4-yl)methylene)acetohydrazide (9f)

White powder; yield: 81%, mp 260–262 °C. IR (KBr, cm^{-1}): 3438 (N—H), 3055 (C—H), 1684 (C═O), 1660 (C═O), 1638 (C═N). ^{1}H NMR (400 MHz, DMSO-d_6, mixture of two isomers E:Z = 61%:39%) δ 11.84 (s, 1H, NH), 11.63 (s, 1H, NH), 9.15 (s, 1H, H_5-pyr), 9.04 (s, 1H, H_5-pyr), [8.52—8.44 (m, 1H), 8.43–8.38 (m, 1H), 8.31–8.23 (m, 2H), 8.05–7.97 (m, 6H), 7.90–7.82 (m, 2H), 7.75–7.68 (m, 1H), 7.61–7.49 (m, 4H), 7.43–7.37 (m, 1H)] (18H, Ar—H and CH═N), 5.57 (s, 2H, CH_2), 5.27 (s, 2H, CH_2). ^{13}C NMR (101 MHz, DMSO, mixture of two isomers) δ 167.8, 165.9, 163.3, 157.5, 151.2, 149.5, 138.8, 136.6, 135.9, 135.7, 135.6, 134.6, 129.7, 129.6, 129.6, 129.2, 129.2, 129.1, 128.6, 128.2, 127.6, 127.5, 127.1, 125.4, 125.3, 125.3, 123.5, 123.3, 118.8, 118.7, 117.1, 114.3, 64.6, 63.3. Anal. Calcd for $C_{33}H_{22}ClF_3N_6O_2$: C, 63.21; H, 3.54; N, 13.40. Found: C, 63.44; H, 3.21; N, 13.82.

4.5.7. 2-(2-(4-Chlorophenyl)-4-oxoquinazolin-3(4H)-yl)-N′-((3-(4-fluorophenyl)-1-phenyl-1H-pyrazol-4-yl)methylene)acetohydrazide (9g)

White powder; yield: 85%, mp 259–261 °C. IR (KBr, cm^{-1}): 3448 (N—H), 3047 (C—H), 1670 (C═O), 1650 (C═O), 1641 (C═N). ^{1}H NMR (400 MHz, DMSO-d_6, mixture of two isomers E:Z = 59%:41%) δ 11.91 (s, 1H, NH), 11.70 (s, 1H, NH), 9.19 (s, 1H, H_5-pyr), 9.07 (s, 1H, H_5-pyr), [8.58–8.49 (m, 2H), 8.40–8.27 (m, 2H), 8.10–8.06 (m, 4H), 7.95–7.88 (m, 2H), 7.82–7.78 (m, 1H), 7.68–7.55 (m, 4H), 7.51–7.38 (m, 3H)] (18H, Ar—H and CH═N), 5.74 (s, 2H, CH_2), 5.34 (s, 2H, CH_2). ^{13}C NMR (101 MHz, DMSO, mixture of two isomers) δ 167.8, 165.9, 165.7, 163.4, 163.2, 161.0, 157.5, 151.2, 150.7, 150.1, 140.5, 138.9, 136.9, 135.9, 135.8, 135.7, 135.6, 134.6, 130.6, 130.6, 130.5, 130.5, 129.7, 129.6, 129.6, 129.5, 128.7, 128.7, 128.6, 128.5, 127.6, 127.5, 126.9, 123.5, 123.3, 118.7, 118.6, 116.6, 116.5, 115.7, 115.5, 115.3, 114.3, 64.6, 63.4. Anal. Calcd for $C_{32}H_{22}ClFN_6O_2$: C, 66.61; H, 3.84; N, 14.56. Found: C, 66.18; H, 3.29; N, 14.

4.5.8. N′-((3-(4-chlorophenyl)-1-phenyl-1H-pyrazol-4-yl)methylene)-2-(2-(4-chlorophenyl)-4-oxoquinazolin-3(4H)-yl)acetohydrazide (9 h)

White powder; yield: 79%, mp 263–265 °C. IR (KBr, cm^{-1}): 3456 (N—H), 3100 (C—H), 1683 (C═O), 1662 (C═O), 1650 (C═N). ^{1}H NMR (400 MHz, DMSO-d_6, mixture of two isomers E:Z = 57%:43%) δ 11.70 (br s, 1H, NH), 9.11 (s, 1H, H_5-pyr), 8.98 (s, 1H, H_5-pyr), [8.51–8.37 (m, 2H), 8.31–8.19 (m, 2H), 8.07–7.93 (m, 4H), 7.85–7.89 (m, 2H), 7.74–7.70 (m, 1H), 7.61–7.47 (m, 6H), 7.42–7.33 (m, 1H)] (18H, Ar—H and CH═N), 5.65 (s, 2H, CH_2), 5.25 (s, 2H, CH_2). ^{13}C NMR (101 MHz, DMSO, mixture of two isomers) δ 167.9, 166.0, 165.8, 157.5, 151.2, 150.3, 149.8, 140.2, 138.8, 136.8, 135.9, 135.9, 135.6, 134.6, 133.3, 133.2, 131.1, 130.1, 130.0, 129.7, 129.6, 129.6, 129.5, 128.9, 128.6, 128.6, 128.5, 128.5, 127.7, 127.6, 127.5, 127.0, 123.5, 123.3, 118.7, 118.6, 116.8, 114.3, 64.7, 63.5. Anal. Calcd for $C_{32}H_{22}Cl_2N6O_2$: C, 64.76; H, 3.74; N, 14.16. Found: C, 64.36; H, 3.32; N, 14.56.

4.5.9. N′-((3-(4-bromophenyl)-1-phenyl-1H-pyrazol-4-yl)methylene)-2-(2-(4-chlorophenyl)-4-oxoquinazolin-3(4H)-yl)acetohydrazide (9i)

White powder; yield: 83%, mp 271–273 °C. IR (KBr, cm^{-1}): 3446 (N—H), 3060 (C—H), 1680 (C═O), 1660 (C═O), 1646 (C═N). ^{1}H NMR (400 MHz, DMSO-d_{6+}, mixture of two isomers E:Z = 62%:38%) δ 11.83 (s, 1H, NH), 11.62 (s, 1H, NH), 9.11 (s, 1H, H_5-pyr), 9.00 (s, 1H, H_5-pyr), [8.50–8.41 (m, 2H), 8.32–8.19 (m, 2H), 8.05–7.94 (m, 4H), 7.81–7.66 (m, 5H), 7.59–7.47 (m, 4H), 7.41–7.36 (m, 1H)] (18H, Ar—H and CH═N), 5.64 (s, 2H, CH_2), 5.26 (s, 2H, CH_2). ^{13}C NMR (101 MHz, DMSO, mixture of two isomers) δ 167.8, 165.9, 165.7, 163.2, 157.5, 151.2, 150.4, 149.8, 140.4, 138.8, 136.8, 135.9, 135.8, 135.7, 135.6, 134.6, 131.6, 131.5, 131.4, 131.1, 130.4, 130.4, 129.7, 129.6, 129.6, 129.5, 129.0, 128.6, 127.9, 127.6, 127.5, 127.0, 123.5, 123.3, 122.0, 121.9, 118.8, 118.6, 116.8, 116.6, 114.3, 64.6, 63.4. Anal. Calcd for $C_{32}H_{22}BrClN_6O_2$: C, 60.25; H, 3.48; N, 13.17. Found: C, 59.98; H, 3.71; N, 13.37.

4.5.10. 2-(2-(4-Chlorophenyl)-4-oxoquinazolin-3(4H)-yl)-N′-((3-phenyl-1-p-tolyl-1H-pyrazol-4-yl)methylene)acetohydrazide (9j)

White powder; yield: 78%, mp 282–285 °C. IR (KBr, cm^{-1}): 3438 (N—H), 3095 (C—H), 1681 (C═O), 1673 (C═O), 1649 (C═N). ^{1}H NMR (400 MHz, DMSO-d_6, mixture of two isomers E:Z = 60%:40%) δ 11.93 (s, 1H, NH), 11.71 (s, 1H, NH), 9.17 (s, 1H, H_5-pyr), 9.04 (s, 1H, H_5-pyr), [8.63–8.51 (m, 2H), 8.42–8.31 (m, 2H), 8.13–8.10 (m, 2H), 8.01–7.98 (m, 2H), 7.89–7.80 (m, 3H), 7.70–7.52 (m, 5H), 7.48–7.42 (m, 2H)] (18H, Ar—H and CH═N), 5.78 (s, 2H, CH_2), 5.36 (s, 2H, CH_2), 2.48 (s, 3H, CH_3), 2.46 (s, 3H, CH_3). ^{13}C NMR (101 MHz, DMSO, mixture of two isomers) δ 167.8, 165.9, 165.7, 163.1, 157.5, 151.6, 151.2, 150.9, 140.7, 137.1, 136.7, 136.3, 135.9, 135.8, 135.7, 135.6, 134.6, 132.2, 131.9, 129.9, 129.9, 129.7, 129.6, 128.7, 128.6, 128.5, 128.5, 128.5, 128.4, 128.3, 128.0, 127.6, 127.5, 126.9, 123.5, 123.3, 118.7, 118.5, 116.5, 116.3, 114.3, 114.3, 64.6, 63.5, 20.4. Anal. Calcd for $C_{33}H_{25}ClN_6O_2$: C, 69.17; H, 4.40; N, 14.67. Found: C, 69.42; H, 4.59; N, 14.26.

4.5.11. 2-(2-(4-Chlorophenyl)-4-oxoquinazolin-3(4H)-yl)-N′-((1,3-dip-tolyl-1H-pyrazol-4-yl)methylene)acetohydrazide (9k)

White powder; yield: 82%, mp 266–268 °C. IR (KBr, cm^{-1}): 3458 (N—H), 3022 (C—H), 1694 (C═O), 1653 (C═O), 1643 (C═N). ^{1}H NMR (400 MHz, DMSO-d_6, mixture of two isomers E:Z = 58%:42%) δ 11.80 (s, 1H, NH), 11.59 (s, 1H, NH), 9.03 (s, 1H, H_5-pyr), 8.90 (s, 1H, H_5-pyr), [8.51–8.42 (m, 3H), 8.32–8.20 (m, 2H), 8.03–7.99 (m, 2H), 7.87 (d, J = 8.4 Hz, 2H), 7.75–7.71 (m, 1H), 7.67–7.60 (m, 2H), 7.54–7.48 (m, 2H), 7.38–7.30 (m, 4H)] (17H, Ar—H and CH═NCH═N), 5.70 (s, 2H, CH_2), 5.25 (s, 2H, CH_2), 2.40 (s, 3H, CH_3), 2.36 (s, 3H, CH_3), 2.35 (s, 3H, CH_3), 2.33 (s, 3H, CH_3). ^{13}C NMR (101 MHz, DMSO, mixture of two isomers) δ 167.8, 165.9, 165.7, 163.1, 157.5, 151.6, 151.2, 151.0, 140.9, 138.0, 137.9, 137.2, 136.7, 136.2, 135.9, 135.8, 135.7, 135.6, 134.6, 129.9,

129.8, 129.7, 129.6, 129.3, 129.2, 129.1, 128.7, 128.5, 128.5, 128.4, 128.2, 127.8, 127.6, 127.5, 126.8, 123.5, 123.3, 118.6, 118.4, 116.4, 116.2, 114.3, 114.3, 64.6, 63.5, 20.8, 20.8, 20.4. Anal. Calcd for $C_{34}H_{27}ClN_6O_2$: C, 69.56; H, 4.64; N, 14.32. Found: C, 69.81; H, 4.21; N, 14.61.

4.5.12. 2-(2-(4-Chlorophenyl)-4-oxoquinazolin-3(4H)-yl)-N′-((3-(4-methoxyphenyl)-1-p-tolyl-1H-pyrazol-4-yl)methylene)acetohydrazide (9l)

White powder; yield: 78%, mp 275–277 °C. IR (KBr, cm^{-1}): 3462 (N—H), 3018(C—H), 1682 (C═O), 1651 (C═O), 1648 (C═N). ^{1}H NMR (400 MHz, DMSO-d_6, mixture of two isomers E:Z = 60%:40%) δ 11.91 (s, 1H, NH), 11.69 (s, 1H, NH), 9.11 (s, 1H, H_5-pyr), 8.98 (s, 1H, H_5-pyr), [8.60–8.52 (m, 2H), 8.44–8.24 (m, 2H), 8.11 (s, 2H), 7.96 (d, J = 8.0 Hz, 2H), 7.82–7.85 (m, 3H), 7.60 (d, J = 8.1 Hz, 2H), 7.49–7.35 (m, 2H), 7.25–7.10 (m, 2H)] (17H, Ar—H and CH═N), 5.79 (s, 2H, CH_2), 5.34 (s, 2H, CH_2), 3.93 (s, 3H, OCH_3), 3.85 (s, 3H, OCH_3), 2.45 (s, 3H, CH_3). ^{13}C NMR (101 MHz, DMSO, mixture of two isomers) δ 167.8, 166.0, 165.7, 163.1, 159.5, 159.4, 157.5, 151.4, 151.2, 150.8, 140.9, 137.3, 136.7, 136.1, 135.9, 135.8, 135.7, 135.6, 134.6, 129.9, 129.8, 129.7, 129.6, 129.6, 129.6, 128.6, 128.5, 127.9, 127.6, 127.5, 126.9, 124.6, 124.3, 123.5, 123.3, 118.6, 118.4, 116.2, 116.0, 114.3, 114.3, 114.1, 113.9, 64.6, 63.5, 55.2, 55.1, 20.4. Anal. Calcd for $C_{34}H_{27}ClN_6O_3$: C, 67.71; H, 4.51; N, 13.94. Found: C, 67.41; H, 4.83; N, 13.25.

4.5.13. 2-(2-(4-Chlorophenyl)-4-oxoquinazolin-3(4H)-yl)-N′-((3-(4-hydroxyphenyl)-1-p-tolyl-1H-pyrazol-4-yl)methylene)acetohydrazide (9m)

White powder; yield: 75%, mp 265–267 °C. IR (KBr, cm^{-1}): 3435 (N—H), 2972 (C—H), 1689 (C═O), 1641 (C═O), 1639 (C═N). ^{1}H NMR (400 MHz, DMSO-d_6, mixture of two isomers E:Z = 57%:43%) δ 11.79 (s, 1H, NH), 11.55 (s, 1H, NH), 8.98 (s, 1H, H_5-pyr), 8.85 (s, 1H, H_5-pyr), [8.52–8.38 (m, 2H), 8.33–8.17 (m, 2H), 8.02 (d, J = 3.4 Hz, 2H), 7.85 (d, J = 8.5 Hz, 2H), 7.75–7.71 (m, 1H), 7.63–7.47 (m, 4H), 7.35–7.30 (m, 2H), 6.94–6.88 (m, 2H)] (17H, Ar—H and CH═N), 5.71 (s, 2H, CH_2), 5.25 (s, 2H, CH_2), 2.36 (s, 3H, CH_3), 2.34 (s, 3H, CH_3). ^{13}C NMR (101 MHz, DMSO, mixture of two isomers) δ 167.7, 166.0, 163.1, 157.9, 157.8, 157.5, 151.9, 151.2, 141.1, 137.5, 136.8, 136.1, 135.9, 135.7, 135.6, 134.6, 129.9, 129.8, 129.7, 129.7, 129.6, 129.6, 128.6, 128.5, 127.7, 127.6, 127.5, 126.6, 123.5, 123.3, 122.9, 118.5, 118.3, 116.0, 115.8, 115.5, 115.2, 114.3, 64.6, 63.5, 20.4. Anal. Calcd for $C_{33}H_{25}ClN_6O_3$: C, 67.29; H, 4.28; N, 14.27. Found: C, 66.81; H, 4.52; N, 14.73.

4.5.14. 2-(2-(4-Chlorophenyl)-4-oxoquinazolin-3(4H)-yl)-N′-((3-(4-nitrophenyl)-1-p-tolyl-1H-pyrazol-4-yl)methylene)acetohydrazide (9n)

White powder; yield: 82%, mp 269–271 °C. IR (KBr, cm^{-1}): 3500 (N—H), 3003 (C—H), 1685 (C═O), 1651 (C═O), 1640 (C═N). ^{1}H NMR (400 MHz, DMSO-d_6, mixture of two isomers E:Z = 59%:41%) δ 12.06 (s, 1H, NH), 11.81 (s, 1H, NH), 9.24 (s, 1H, H_5-pyr), 9.13 (s, 1H, H_5-pyr), [8.64–8.59 (m, 1H), 8.52–8.35 (m, 5H), 8.25–8.22 (m, 1H)8.13–8.10 (m, 3H), 8.02–7.99 (m, 2H), 7.73 (d, J = 8.7 Hz, 1H), 7.65–7.61 (m, 2H), 7.50–7.45 (m, 2H)] (17H, Ar—H and CH═N), 5.73 (s, 2H, CH_2), 5.39 (s, 2H, CH_2), 2.49 (s, 3H, CH_3), 2.48 (s, 3H, CH_3). ^{13}C NMR (101 MHz, DMSO, mixture of two isomers) δ 167.9, 166.1, 165.9, 163.3, 157.5, 151.2, 148.3, 147.0, 140.0, 138.9, 136.8, 136.6, 136.5, 135.9, 135.6, 134.6, 134.5, 130.0, 129.7, 129.7, 129.5, 129.4, 129.4, 128.6, 128.6, 127.6, 127.5, 127.4, 127.3, 123.8, 123.7, 123.6, 123.3, 118.8, 118.6, 117.2, 114.3, 64.2, 63.4, 20.4. Anal. Calcd for $C_{33}H_{24}ClN_7O_4$: C, 64.13; H, 3.91; N, 15.86. Found: C, 64.48; H, 3.65; N, 16.22.

4.5.15. N′-((3-(4-chlorophenyl)-1-p-tolyl-1H-pyrazol-4-yl)methylene)-2-(2-(4-chlorophenyl)-4-oxoquinazolin-3(4H)-yl)acetohydrazide (9o)

White powder; yield: 75%, mp 272–274 °C. IR (KBr, cm^{-1}): 3456 (N—H), 3132 (C—H), 1683 (C═O), 1662 (C═O), 1648 (C═N). ^{1}H NMR (400 MHz, DMSO-d_6, mixture of two isomers E:Z = 58%:42%) δ 11.86 (br s, 1H, NH), 9.18 (s, 1H, H_5-pyr), 9.03 (s, 1H, H_5-pyr), [8.60–8.49 (m, 2H), 8.42–8.30 (m, 2H), 8.14–8.00 (m, 2H), 8.01–7.88 (m, 4H), 7.86–7.83 (m, 1H), 7.72–7.60 (m, 4H), 7.48–7.42 (m, 2H)] (17H, Ar—HAr—H and CH═N), 5.77 (s, 2H, CH_2), 5.36 (s, 2H, CH_2), 2.48 (s, 3H, CH_3), 2.46 (s, 3H, CH_3). ^{13}C NMR (101 MHz, DMSO, mixture of two isomers) δ 167.9, 166.0, 157.5, 151.2, 149.5, 136.8, 136.6, 136.4, 135.9, 135.6, 134.6, 133.1, 131.2, 130.9, 130.1, 130.0, 129.9, 129.9, 129.7, 129.6, 128.6, 128.6, 128.5, 128.5, 127.6, 127.5, 123.5, 123.3, 118.6, 118.5, 116.6, 114.3, 63.5, 20.4. Anal. Calcd for $C_{33}H_{24}Cl_2N_6O_2$: C, 65.24; H, 3.98; N, 13.83. Found: C, 65.66; H, 4.23; N, 14.32.

4.5.16. N′-((3-(4-bromophenyl)-1-p-tolyl-1H-pyrazol-4-yl)methylene)-2-(2-(4-chlorophenyl)-4-oxoquinazolin-3(4H)-yl)acetohydrazide (9p)

White powder; yield: 81%, mp 281–283 °C. IR (KBr, cm^{-1}): 3477 (N—H), 3142 (C—H),1683 (C═O), 1645 (C═O), 1639 (C═N). ^{1}H NMR (400 MHz, DMSO-d_6, mixture of two isomers E:Z = 61%:39%) δ 11.83 (s, 1H, NH), 11.61 (s, 1H, NH), 9.05 (s, 1H, H_5-pyr), 8.93 (s, 1H, H_5-pyr), [8.51–8.38 (m, 2H), 8.32–8.18 (m, 2H), 8.01 (d, J = 3.6 Hz, 2H), 7.89–7.83 (m, 2H), 7.78–7.66 (m, 5H), 7.53–7.50 (m, 2H), 7.36–7.31 (m, 2H)] (17H, Ar—H and CH═N), 5.64 (s, 2H, CH_2), 5.26 (s, 2H, CH_2), 2.36 (s, 3H, CH_3), 2.35 (s, 3H, CH_3). ^{13}C NMR (101 MHz, DMSO, mixture of two isomers) δ 167.8, 165.9, 165.7, 157.5, 151.2, 149.6, 140.5, 136.9, 136.6, 136.4, 135.9, 135.6, 134.6, 131.6, 131.4, 130.4, 130.3, 129.9, 129.9, 129.7, 129.6, 128.7, 128.6, 127.6, 127.5, 123.3, 121.8, 118.7, 118.5, 116.6, 114.3, 63.4, 20.4. Anal. Calcd for $C_{33}H_{24}BrClN_6O_2$: C, 60.80; H, 3.71; N, 12.89. Found: C, 60.52; H, 4.11; N, 12.52.

4.6. α-Glucosidase inhibition assay

The α-glucosidase inhibition property of quinazolinone-pyrazole 9a-p were determined according to the previously reported method [66]. The α-glucosidase enzyme ((EC3.2.1.20, Saccharomyces cerevisiae, 20 U/mg) and p-nitrophenyl glucopyranoside as substrate were purchased from Sigma-Aldrich. Enzyme and desired concentrations of nitrophenol-α-D-glycopyranoside (PNP) were stored in potassium phosphate buffer (pH 6.8). The standard and all tested compounds were dissolved in DMSO (10 mM) and further diluted with potassium phosphate buffer for subsequent use in the enzyme inhibition assay (10% final concentration).

Firstly, a mixture containing phosphate buffer phosphate (135 μL, pH 6.8,50 mM), various concentrations of tested compounds 9a-p (20 μL) and enzyme solution (20 μL) were added to the 96-well plate and pre-incubated at 37 °C for 10 min. Then, 25 μL of 4 mM of *p*-nitrophenyl glucopyranoside as substrate was added to each well and incubation was continued at 37 °C for 20 min. Finally, the absorbance change was measured at 405 nm using a spectrophotometer (Gen5, Power wave xs2, BioTek, America). DMSO and acarbose were used as the control and standard inhibitor, respectively. The percentage of inhibition for target compounds, control, and the standard inhibitor was calculated by using the following formula:

$$\%\text{Inhibition} = [(\text{Abs control} - \text{Abs sample})/\text{Abs control}] \times 100$$

IC50 values of tested compounds were obtained from the nonlinear regression curve (logit method). All experiments were performed in triplicate and the results are expressed as the mean ± SD.

4.7. Kinetics of enzyme inhibition

The kinetic analysis was performed under the above-mentioned reaction condition. The mode of inhibition of the most active compound 9i was investigated by varying the concentration of *p*-nitrophenyl α-D-glucopyranoside as substrate in the absence and presence of compound 9i at different concentrations. The enzyme solution (1 U/mL, 20 μL) was incubated with different concentrations of 0, 20, 40, and 60 μM of the most potent compound 9i (20 μL) for 15 min at 30 °C. The change in the absorbance was measured at 405 nm for 20 min using a spectrophotometer (Gen5, Power wave xs2, BioTek, America) following addition increasing concentrations of p-nitrophenyl glucopyranoside (2–10 mM)

as substrate. A Lineweaver–Burk plot was generated to identify the type of inhibition and the Michaelis–Menten constant (Km) value was determined from the plot between reciprocal of the substrate concentration (1/[S]) and reciprocal of enzyme rate (1/V) over various inhibitor concentrations. The experimental inhibitor constant (K_i) value was constructed by secondary plots of the inhibitor concentration [I] versus Km.

4.8. In vitro α-amylase inhibition assay

The anti-α-amylase activity of the compounds 9i, 9g, and 9k was determined based on the colorimetric method described by Taha et al. [17].

4.9. Molecular docking

Docking studies were performed using genetic algorithm-based docking program (GOLD) implemented in the Discovery Studio 4.1 (Accelrys Software Inc.) to study the binding modes and important interactions of some selected synthesized compounds. The 3D structure of compounds has been drawn by using Chem Draw Ultra 12.0 software. The Ligand structures were transferred into Discovery Studio (DS), typed with CHARMm force field and partial charges were calculated by Momany-Rone option. Subsequently, the resulting structures were minimized with Smart Minimizer algorithm, which performs 1000 steps of steepest descent with a RMS gradient tolerance of 3, followed by Conjugate Gradient minimization. The 3D Modeled structure of the α-glucosidase was prepared using the protein preparation protocol of DS. In this step, complex typed with CHARMm force field, hydrogen atoms were added, all water molecules were removed and pH adjusted to neutral 7.4. A 9 Å radius sphere was defined as the binding region for docking study. Other parameters were set by default protocol settings. Selected synthesized compounds were docked into the active site of the α-glucosidase and 10 different conformations for each compound were ranked by GOLD score. Finally, the pose with the best GOLD score was selected to analyze the mode of binding.

4.10. Molecular dynamic simulation

Molecular dynamic (MD) simulation of this study was performed by using the Desmond module implemented in Maestro interface (from Schrödinger 2018-4 suite). In order to build the system for MD simulation, the protein–ligand complexes were solvated with SPC explicit water molecules and placed in the center of an orthorhombic box of appropriate size in the Periodic Boundary Condition. Sufficient counterions and a 0.15 M solution of NaCl were also utilized to neutralize the system and to simulate the real cellular ionic concentrations, respectively. The MD protocol involved minimization, pre-production, and finally production MD simulation steps. In the minimization procedure, the entire system was allowed to relax for 2500 steps by the steepest descent approach. Then the temperature of the system was raised from 0 to 300 K with a small force constant on the enzyme in order to restrict any drastic changes. MD simulations were performed via NPT (constant number of atoms, constant pressure i.e. 1.01325 bar and constant temperature i.e. 300 K) ensemble. The Nose-Hoover chain method was used as the default thermostat with 1.0 ps interval and Martyna-Tobias-Klein as the default barostat with 2.0 ps interval by applying isotropic coupling style. Long-range electrostatic forces were calculated based on Particle-mesh-based Ewald approach with the cut-off radius for columbic forces set to 9.0 Å. Finally, the system subjected to produce MD simulations for 20 ns for protein–ligand complex. During the simulation every 1000 ps of the actual frame was stored. The dynamic behavior and structural changes of the systems were analyzed by the calculation of the root mean square deviation (RMSD) and RMSF. Subsequently, the energy-minimized structure calculated from the equilibrated trajectory system was evaluated for investigation of each ligand–protein complex interaction.

4.11. Prime MM-GBSA

The ligand-binding energies (ΔG_{Bind}) were calculated for the best active compound and acarbose using Molecular mechanics/generalized born surface area (MM–GBSA) modules (Schrödinger LLC 2018) based on the following equation:

$$\Delta G_{Bind} = E_{Complex} - \left[E_{Receptor} + E_{Ligand}\right]$$

where ΔG_{Bind} is the calculated relative free energy which includes both ligand and receptor strain energy. $E_{Complex}$ is the MM-GBSA energy of the minimized complex, and E_{Ligand} is the MM-GBSA energy of the ligand after removing it from the complex and allowing it to relax. $E_{Receptor}$ is the MM-GBSA energy of relaxed protein after separating it from the ligand. The MM-GBSA calculation was performed by extracting the total number of 102 snapshots from the last 5 ns trajectory (production phase) with the snapshot interval of 50 ps for binding free energy calculation.

Declaration of Competing Interest

The authors declare that they have no known competing financial interests or personal relationships that could have appeared to influence the work reported in this paper.

Appendix A. Supplementary material

Supplementary data to this article can be found online at https://doi.org/10.1016/j.bioorg.2021.105127.

References

[1] A.J. Hirsh, S. Yao, J.D. Young, C.I. Cheeseman, Inhibition of glucose absorption in the rat jejunum: a novel action of alpha-D-glucosidase inhibitors, Gastroenterology 113 (1) (1997) 205–211.
[2] A.J. Scheen, Is there a role for α-glucosidase inhibitors in the prevention of type 2 diabetes mellitus? Drugs 63 (10) (2003) 933–951.
[3] F.A. van de Laar, Alpha-glucosidase inhibitors in the early treatment of type 2 diabetes, Vasc. Health Risk Manage. 4 (6) (2008) 1189.
[4] S.R. Joshi, E. Standl, N. Tong, P. Shah, S. Kalra, R. Rathod, Therapeutic potential of α-glucosidase inhibitors in type 2 diabetes mellitus: an evidence-based review, Expert Opin. Pharmacother. 16 (13) (2015) 1959–1981.
[5] R. Pili, J. Chang, R.A. Partis, R.A. Mueller, F.J. Chrest, A. Passaniti, The α-glucosidase I inhibitor castanospermine alters endothelial cell glycosylation, prevents angiogenesis, and inhibits tumor growth, Cancer Res. 55 (13) (1995) 2920–2926.
[6] N. Zitzmann, A.S. Mehta, S. Carrouée, T.D. Butters, F.M. Platt, J. McCauley, B. S. Blumberg, R.A. Dwek, T.M. Block, Imino sugars inhibit the formation and secretion of bovine viral diarrhea virus, a pestivirus model of hepatitis C virus: implications for the development of broad spectrum anti-hepatitis virus agents, Proc. Natl. Acad. Sci. 96 (21) (1999) 11878–11882.
[7] A. Mehta, N. Zitzmann, P.M. Rudd, T.M. Block, R.A. Dwek, α-Glucosidase inhibitors as potential broad based anti-viral agents, FEBS Lett. 430 (1–2) (1998) 17–22.
[8] A.J. Rawlings, H. Lomas, A.W. Pilling, M.J.R. Lee, D.S. Alonzi, J.S. Rountree, S. F. Jenkinson, G.W. Fleet, R.A. Dwek, J.H. Jones, Synthesis and Biological Characterisation of Novel N-Alkyl-Deoxynojirimycin α-Glucosidase Inhibitors, ChemBioChem 10 (6) (2009) 1101–1105.
[9] H. Bischoff, Pharmacology of alpha-glucosidase inhibition, Eur. J. Clin. Invest. 24 (1994) 3–10.
[10] M. Toeller, α-Glucosidase inhibitors in diabetes: efficacy in NIDDM subjects, Eur. J. Clin. Invest. 24 (S3) (1994) 31–35.
[11] P. Hollander, Safety profile of acarbose, an α-glucosidase inhibitor, Drugs 44 (3) (1992) 47–53.
[12] M. Özil, M. Emirik, S.Y. Etlik, S. Ülker, B. Kahveci, A simple and efficient synthesis of novel inhibitors of alpha-glucosidase based on benzimidazole skeleton and molecular docking studies, Bioorg. Chem. 68 (2016) 226–235.
[13] T. Luthra, V. Banothu, U. Adepally, K. Kumar, M. Swathi, S. Chakrabarti, S. R. Maddi, S. Sen, Discovery of novel pyrido-pyrrolidine hybrid compounds as alpha-glucosidase inhibitors and alternative agent for control of type 1 diabetes, Eur. J. Med. Chem. 188 (2020), 112034.
[14] X.-T. Xu, X.-Y. Deng, J. Chen, Q.-M. Liang, K. Zhang, D.-L. Li, P.-P. Wu, X. Zheng, R.-P. Zhou, Z.-Y. Jiang, Synthesis and biological evaluation of coumarin derivatives as α-glucosidase inhibitors, Eur. J. Med. Chem. 189 (2020), 112013.
[15] M. Taha, S. Imran, M. Salahuddin, N. Iqbal, F. Rahim, N. Uddin, A. Shehzad, R. K. Farooq, M. Alomari, K.M. Khan, Evaluation and docking of indole sulfonamide

as a potent inhibitor of α-glucosidase enzyme in streptozotocin–induced diabetic albino wistar rats, Bioorg. Chem. 110 (2021), 104808.
[16] M.T. Javid, F. Rahim, M. Taha, H.U. Rehman, M. Nawaz, S. Imran, I. Uddin, A. Mosaddik, K.M. Khan, Synthesis, in vitro α-glucosidase inhibitory potential and molecular docking study of thiadiazole analogs, Bioorg. Chem. 78 (2018) 201–209.
[17] M. Taha, S.A.A. Shah, M. Afifi, S. Imran, S. Sultan, F. Rahim, K.M. Khan, Synthesis, α-glucosidase inhibition and molecular docking study of coumarin based derivatives, Bioorg. Chem. 77 (2018) 586–592.
[18] M. Taha, S. Imran, F. Rahim, A. Wadood, K.M. Khan, Oxindole based oxadiazole hybrid analogs: Novel α-glucosidase inhibitors, Bioorg. Chem. 76 (2018) 273–280.
[19] Y.T. Han, K. Kim, G.-I. Choi, H. An, D. Son, H. Kim, H.-J. Ha, J.-H. Son, S.-J. Chung, H.-J. Park, Pyrazole-5-carboxamides, novel inhibitors of receptor for advanced glycation end products (RAGE), Eur. J. Med. Chem. 79 (2014) 128–142.
[20] Y. Zou, L. Xu, W. Chen, Y. Zhu, T. Chen, Y. Fu, L. Li, L. Ma, B. Xiong, X. Wang, Discovery of pyrazole as C-terminus of selective BACE1 inhibitors, Eur. J. Med. Chem. 68 (2013) 270–283.
[21] V. Aware, N. Gaikwad, S. Chavan, S. Manohar, J. Bose, S. Khanna, B.-R. Chandrika, N. Dixit, K.S. Singh, A. Damre, Cyclopentyl-pyrimidine based analogues as novel and potent IGF-1R inhibitor, Eur. J. Med. Chem. 92 (2015) 246–256.
[22] A. Kamal, A.B. Shaik, S. Polepalli, G.B. Kumar, V.S. Reddy, R. Mahesh, S. Garimella, N. Jain, Synthesis of arylpyrazole linked benzimidazole conjugates as potential microtubule disruptors, Bioorg. Med. Chem. 23 (5) (2015) 1082–1095.
[23] S. Kantevari, D. Addla, P.K. Bagul, B. Sridhar, S.K. Banerjee, Synthesis and evaluation of novel 2-butyl-4-chloro-1-methylimidazole embedded chalcones and pyrazoles as angiotensin converting enzyme (ACE) inhibitors, Bioorg. Med. Chem. 19 (16) (2011) 4772–4781.
[24] Y.-R. Li, C. Li, J.-C. Liu, M. Guo, T.-Y. Zhang, L.-P. Sun, C.-J. Zheng, H.-R. Piao, Synthesis and biological evaluation of 1, 3-diaryl pyrazole derivatives as potential antibacterial and anti-inflammatory agents, Bioorg. Med. Chem. Lett. 25 (22) (2015) 5052–5057.
[25] T. Wang, D. Banerjee, T. Bohnert, J. Chao, I. Enyedy, J. Fontenot, K. Guertin, H. Jones, E.Y. Lin, D. Marcotte, Discovery of novel pyrazole-containing benzamides as potent RORγ inverse agonists, Bioorg. Med. Chem. Lett. 25 (15) (2015) 2985–2990.
[26] B.V. Kendre, M.G. Landge, S.R. Bhusare, Synthesis and biological evaluation of some novel pyrazole, isoxazole, benzoxazepine, benzothiazepine and benzodiazepine derivatives bearing an aryl sulfonate moiety as antimicrobial and anti-inflammatory agents, Arabian J. Chem. 12 (8) (2019) 2091–2097.
[27] L.-G. Yu, T.-F. Ni, W. Gao, Y. He, Y.-Y. Wang, H.-W. Cui, C.-G. Yang, W.-W. Qiu, The synthesis and antibacterial activity of pyrazole-fused tricyclic diterpene derivatives, Eur. J. Med. Chem. 90 (2015) 10–20.
[28] R. Prasath, P. Bhavana, S. Sarveswari, S.W. Ng, E.R. Tiekink, Efficient ultrasound-assisted synthesis, spectroscopic, crystallographic and biological investigations of pyrazole-appended quinolinyl chalcones, J. Mol. Struct. 1081 (2015) 201–210.
[29] M. Khoobi, F. Ghanoni, H. Nadri, A. Moradi, M.P. Hamedani, F.H. Moghadam, S. Emami, M. Vosooghi, R. Zadmard, A. Foroumadi, New tetracyclic tacrine analogs containing pyrano [2, 3-c] pyrazole: efficient synthesis, biological assessment and docking simulation study, Eur. J. Med. Chem. 89 (2015) 296–303.
[30] D. Manvar, S. Pelliccia, G. La Regina, V. Famiglini, A. Coluccia, A. Ruggieri, S. Anticoli, J.-C. Lee, A. Basu, O. Cevik, New 1-phenyl-5-(1H-pyrrol-1-yl)-1H-pyrazole-3-carboxamides inhibit hepatitis C virus replication via suppression of cyclooxygenase-2, Eur. J. Med. Chem. 90 (2015) 497–506.
[31] P.N. Kalaria, S.P. Satasia, J.R. Avalani, D.K. Raval, Ultrasound-assisted one-pot four-component synthesis of novel 2-amino-3-cyanopyridine derivatives bearing 5-imidazopyrazole scaffold and their biological broadcast, Eur. J. Med. Chem. 83 (2014) 655–664.
[32] M.F. Khan, M.M. Alam, G. Verma, W. Akhtar, M. Akhter, M. Shaquiquzzaman, The therapeutic voyage of pyrazole and its analogs: a review, Eur. J. Med. Chem. 120 (2016) 170–201.
[33] K. Kees, J. Fitzgerald Jr, K. Steiner, J. Mattes, B. Mihan, T. Tosi, D. Mondoro, M. L. McCaleb, New Potent Antihyperglyceimc Agents in db/db Mice: Synthesis and Structure-Activity Relationship Studies of (4-substitutedbenzyl)-(trifluoromethyl) pyrazoles and-pyrazolones, J. Med. Chem 39 (1996) 3920–3928.
[34] S. Shu, X. Cai, J. Li, Y. Feng, A. Dai, J. Wang, D. Yang, M.-W. Wang, H. Liu, Design, synthesis, structure–activity relationships, and docking studies of pyrazole-containing derivatives as a novel series of potent glucagon receptor antagonists, Bioorg. Med. Chem. 24 (12) (2016) 2852–2863.
[35] S. Shu, A. Dai, J. Wang, B. Wang, Y. Feng, J. Li, X. Cai, D. Yang, D. Ma, M.-W. Wang, A novel series of 4-methyl substituted pyrazole derivatives as potent glucagon receptor antagonists: Design, synthesis and evaluation of biological activities, Bioorg. Med. Chem. 26 (8) (2018) 1896–1908.
[36] F. Chaudhry, S. Naureen, R. Huma, A. Shaukat, M. Al-Rashida, N. Asif, M. Ashraf, M.A. Munawar, M.A. Khan, In search of new α-glucosidase inhibitors: Imidazolylpyrazole derivatives, Bioorg. Chem. 71 (2017) 102–109.
[37] F. Chaudhry, S. Naureen, S. Choudhry, R. Huma, M. Ashraf, M. Al-Rashida, B. Jahan, M.H. Khan, F. Iqbal, M.A. Munawar, Evaluation of α-glucosidase inhibiting potentials with docking calculations of synthesized arylidene-pyrazolones, Bioorg. Chem. 77 (2018) 507–514.
[38] V. Pogaku, K. Gangarapu, S. Basavoju, K.K. Tatapudi, S.B. Katragadda, Design, synthesis, molecular modelling, ADME prediction and anti-hyperglycemic evaluation of new pyrazole-triazolopyrimidine hybrids as potent α-glucosidase inhibitors, Bioorg. Chem. 93 (2019), 103307.
[39] S.K. Sharma, A. Panneerselvam, K. Singh, G. Parmar, P. Gadge, O.C. Swami, Teneligliptin in management of type 2 diabetes mellitus, Diabet. Metabolic Syndrome Obesity: Targets Therapy 9 (2016) 251.
[40] M.E. López-Viseras, B. Fernández, S. Hilfiker, C.S. González, J.L. González, A. J. Calahorro, E. Colacio, A. Rodríguez-Diéguez, In vivo potential antidiabetic activity of a novel zinc coordination compound based on 3-carboxy-pyrazole, J. Inorg. Biochem. 131 (2014) 64–67.
[41] E. Hernández-Vázquez, H. Ocampo-Montalban, L. Cerón-Romero, M. Cruz, J. Gómez-Zamudio, G. Hiriart-Valencia, R. Villalobos-Molina, A. Flores-Flores, S. Estrada-Soto, Antidiabetic, antidyslipidemic and toxicity profile of ENV-2: A potent pyrazole derivative against diabetes and related diseases, Eur. J. Pharmacol. 803 (2017) 159–166.
[42] H. Li, R. Huang, D. Qiu, Z. Yang, X. Liu, J. Ma, Z. Ma, Synthesis and bioactivity of 4-quinazoline oxime ethers, Prog. Nat. Sci. 8 (3) (1998) 359–365.
[43] N. Krishnarth, S.K. Verma, A. Chaudhar, Synthesis and anti-inflammatory activity of some novel quinazolinone derivatives, FABAD J. Pharm. Sci. 45 (3) (2020) 205–210.
[44] S. Farooq, A. Mazhar, N. Ullah, One-pot multicomponent synthesis of novel 3, 4-dihydro-3-methyl-2 (1H)-quinazolinone derivatives and their biological evaluation as potential antioxidants, enzyme inhibitors, antimicrobials, cytotoxic and anti-inflammatory agents, Arabian J. Chem. 13 (12) (2020) 9145–9165.
[45] S. Malasala, J. Gour, M.N. Ahmad, S. Gatadi, M. Shukla, G. Kaul, A. Dasgupta, Y. Madhavi, S. Chopra, S. Nanduri, Copper mediated one-pot synthesis of quinazolinones and exploration of piperazine linked quinazoline derivatives as anti-mycobacterial agents, RSC Adv. 10 (71) (2020) 43533–43538.
[46] A. Suresh, S. Srinivasarao, Y.M. Khetmalis, S. Nizalapur, M. Sankaranarayanan, K. V.G.C. Sekhar, Inhibitors of pantothenate synthetase of Mycobacterium tuberculosis–a medicinal chemist perspective, RSC Adv. 10 (61) (2020) 37098–37115.
[47] T.S. Patel, J.D. Bhatt, R.B. Dixit, C.J. Chudasama, B.D. Patel, B.C. Dixit, Green synthesis, biological evaluation, molecular docking studies and 3D-QSAR analysis of novel phenylalanine linked quinazoline-4 (3H)-one-sulphonamide hybrid entities distorting the malarial reductase activity in folate pathway, Bioorg. Med. Chem. 27 (16) (2019) 3574–3586.
[48] R. Venkatesh, S. Kasaboina, N. Jain, S. Janardhan, U.D. Holagunda, L. Nagarapu, Design and synthesis of novel sulphamide tethered quinazolinone hybrids as potential antitumor agents, J. Mol. Struct. 1181 (2019) 403–411.
[49] M.A.E.-A.M. El, M.S. Salem, S.A.M. Al-Mabrook, Synthesis and anticancer activity of novel quinazolinone and benzamide derivatives, Res. Chem. Intermed. 44 (4) (2018) 2545–2559.
[50] S. Chen, M. Jiang, B. Chen, J. Salaenoi, S.-I. Niaz, J. He, L. Liu, Penicamide A, a unique N, N′-ketal quinazolinone alkaloid from ascidian-derived fungus Penicillium sp. 4829, Mar. Drugs 17 (9) (2019) 522.
[51] S. Zhou, G. Huang, Synthesis of anti-allergic drugs, RSC Adv. 10 (10) (2020) 5874–5885.
[52] H. Jin, H.-G. Dan, G.-W. Rao, Research progress in quinazoline derivatives as multi-target tyrosine kinase inhibitors, Heterocycl. Commun. 24 (1) (2018) 1–10.
[53] Z. Hajimahdi, R. Zabihollahi, M.R. Aghasadeghi, A. Zarghi, Design, Synthesis, Docking Studies and Biological Activities Novel 2, 3-Diaryl-4-Quinazolinone Derivatives as Anti-HIV-1 Agents, Curr. HIV Res. 17 (3) (2019) 214–222.
[54] M.K. Yadav, L. Tripathi, D. Goswami, Evaluation of Anticonvulsant Activity and Toxicity Screening of Semicarbazones Derived from Quinazolinone Scaffold, Curr. Bioact. Compd. 15 (5) (2019) 573–581.
[55] V.G. Ugale, S.B. Bari, S.C. Khadse, P.N. Reddy, C.G. Bonde, P.J. Chaudhari, Exploring Quinazolinones as Anticonvulsants by Molecular Fragmentation Approach: Structural Optimization, Synthesis and Pharmacological Evaluation Studies, ChemistrySelect 5 (10) (2020) 2902–2912.
[56] J. Rudolph, W.P. Esler, S. O'Connor, P.D. Coish, P.L. Wickens, M. Brands, D. E. Bierer, B.T. Bloomquist, G. Bondar, L. Chen, Quinazolinone derivatives as orally available ghrelin receptor antagonists for the treatment of diabetes and obesity, J. Med. Chem. 50 (21) (2007) 5202–5216.
[57] V. Gurram, R. Garlapati, C. Thulluri, N. Madala, K.S. Kasani, P.K. Machiraju, R. Doddapalla, U. Addepally, R. Gundla, B. Patro, Design, synthesis, and biological evaluation of quinazoline derivatives as α-glucosidase inhibitors, Med. Chem. Res. 24 (5) (2015) 2227–2237.
[58] K. Javaid, S.M. Saad, S. Rasheed, S.T. Moin, N. Syed, I. Fatima, U. Salar, K.M. Khan, S. Perveen, M.I. Choudhary, 2-Arylquinazolin-4 (3H)-ones: A new class of α-glucosidase inhibitors, Bioorg. Med. Chem. 23 (23) (2015) 7417–7421.
[59] M. Saeedi, M. Mohammadi-Khanaposhtani, P. Pourrabia, N. Razzaghi, R. Ghadimi, S. Imanparast, M.A. Faramarzi, F. Bandarian, E.N. Esfahani, M. Safavi, Design and synthesis of novel quinazolinone-1, 2, 3-triazole hybrids as new anti-diabetic agents: in vitro α-glucosidase inhibition, kinetic, and docking study, Bioorg. Chem. 83 (2019) 161–169.
[60] M. Wei, W.-M. Chai, R. Wang, Q. Yang, Z. Deng, Y. Peng, Quinazolinone derivatives: synthesis and comparison of inhibitory mechanisms on α-glucosidase, Bioorg. Med. Chem. 25 (4) (2017) 1303–1308.
[61] S. Moghimi, M. Toolabi, S. Salarinejad, L. Firoozpour, S.E.S. Ebrahimi, F. Safari, S. Mojtabavi, M.A. Faramarzi, A. Foroumadi, Design and synthesis of novel pyridazine N-aryl acetamides: In-vitro evaluation of α-glucosidase inhibition, docking, and kinetic studies, Bioorg. Chem. 102 (2020), 104071.
[62] E.S. Gosnell, S. Thikkurissy, Assessment and Management of Pain in the Pediatric Patient, Pediatric Dentistry, Elsevier, 2019, pp. 97-115. e1.
[63] M.U. Ahmad, M. Rafiq, B. Zahra, M. Islam, M. Ashraf, M. Al-Rashida, A. Khan, J. Hussain, Z. Shafiq, A. Al-Harrasi, Synthesis of benzimidazole based hydrazones as non-sugar based α-glucosidase inhibitors: Structure activity relation and molecular docking, Drug Dev. Res. (2021).
[64] S. Khan, M. Tariq, M. Ashraf, S. Abdullah, M. Al-Rashida, M. Khalid, P. Taslimi, M. Fatima, R. Zafar, Z. Shafiq, Probing 2-acetylbenzofuran hydrazones and their metal complexes as α-glucosidase inhibitors, Bioorg. Chem. 102 (2020), 104082.

[65] S. Malik, A. Khan, M.M. Naseer, S.U. Khan, A. Ashraf, M. Ashraf, M. Rafiq, K. Mahmood, M.N. Tahir, Z. Shafiq, Xanthenone-based hydrazones as potent α-glucosidase inhibitors: synthesis, solid state self-assembly and in silico studies, Bioorg. Chem. 84 (2019) 372–383.
[66] M. Adib, F. Peytam, M. Rahmanian-Jazi, S. Mahernia, H.R. Bijanzadeh, M. Jahani, M. Mohammadi-Khanaposhtani, S. Imanparast, M.A. Faramarzi, M. Mahdavi, New 6-amino-pyrido [2, 3-d] pyrimidine-2, 4-diones as novel agents to treat type 2 diabetes: A simple and efficient synthesis, α-glucosidase inhibition, molecular modeling and kinetic study, Eur. J. Med. Chem. 155 (2018) 353–363.
[67] M. Mohammadi-Khanaposhtani, S. Rezaei, R. Khalifeh, S. Imanparast, M. A. Faramarzi, S. Bahadorikhalili, M. Safavi, F. Bandarian, E.N. Esfahani, M. Mahdavi, Design, synthesis, docking study, α-glucosidase inhibition, and cytotoxic activities of acridine linked to thioacetamides as novel agents in treatment of type 2 diabetes, Bioorg. Chem. 80 (2018) 288–295.
[68] Y. Wang, L. Ma, C. Pang, M. Huang, Z. Huang, L. Gu, Synergetic inhibition of genistein and d-glucose on α-glucosidase, Bioorg. Med. Chem. Lett. 14 (11) (2004) 2947–2950.
[69] J.-M.G. Rodriguez, N.P. Hux, S.J. Philips, M.H. Towns, Michaelis-Menten graphs, Lineweaver-Burk plots, and reaction schemes: investigating introductory biochemistry students' conceptions of representations in enzyme kinetics, J. Chem. Educ. 96 (9) (2019) 1833–1845.
[70] D. Shahzad, A. Saeed, F.A. Larik, P.A. Channar, Q. Abbas, M.F. Alajmi, M.I. Arshad, M.F. Erben, M. Hassan, H. Raza, Novel C-2 symmetric molecules as α-glucosidase and α-amylase inhibitors: design, synthesis, kinetic evaluation, molecular docking and pharmacokinetics, Molecules 24 (8) (2019) 1511.
[71] P. Lin, J.-C. Zeng, J.-G. Chen, X.-L. Nie, E. Yuan, X.-Q. Wang, D.-Y. Peng, Z.-P. Yin, Synthesis, in vitro inhibitory activity, kinetic study and molecular docking of novel N-alkyl–deoxynojirimycin derivatives as potential α-glucosidase inhibitors, J. Enzyme Inhib. Med. Chem. 35 (1) (2020) 1879–1890.
[72] F. Payan, Structural basis for the inhibition of mammalian and insect α-amylases by plant protein inhibitors, Biochimica et Biophysica Acta (BBA) – Proteins Proteom. 1696 (2) (2004) 171–180.
[73] F. Azimi, J.B. Ghasemi, H. Azizian, M. Najafi, M.A. Faramarzi, L. Saghaei, H. Sadeghi-Aliabadi, B. Larijani, F. Hassanzadeh, M. Mahdavi, Design and synthesis of novel pyrazole-phenyl semicarbazone derivatives as potential α-glucosidase inhibitor: Kinetics and molecular dynamics simulation study, Int. J. Biol. Macromol. (2020).
[74] S.A. Hollingsworth, R.O. Dror, Molecular dynamics simulation for all, Neuron 99 (6) (2018) 1129–1143.
[75] E. Fuglebakk, J. Echave, N. Reuter, Measuring and comparing structural fluctuation patterns in large protein datasets, Bioinformatics 28 (19) (2012) 2431–2440.
[76] T. Hou, J. Wang, Y. Li, W. Wang, Assessing the performance of the MM/PBSA and MM/GBSA methods. 1. The accuracy of binding free energy calculations based on molecular dynamics simulations, J. Chem. Inf. Model. 51 (1) (2011) 69–82.
[77] T. Hou, J. Wang, Y. Li, W. Wang, Assessing the performance of the MM/PBSA and MM/GBSA methods: II. The accuracy of ranking poses generated from docking, J. Comput. Chem. 32 (5) (2011) 866.
[78] E. Menteşe, N. Karaali, G. Akyüz, F. Yılmaz, S. Ülker, B. Kahveci, Synthesis and evaluation of α-glucosidase and pancreatic lipase inhibition by quinazolinone-coumarin hybrids, Chem. Heterocycl. Compd. 52 (12) (2016) 1017–1024.
[79] R. Pundeer, P. Ranjan, K. Pannu, O. Prakash, One-pot synthesis of some new semicarbazone, thiosemicarbazone, and hydrazone derivatives of 1-phenyl-3-aryl-pyrazole-4-carboxaldehyde from acetophenone phenylhydrazones using Vilsmeier-Haack reagent, Synth. Commun. 39 (2) (2008) 316–324.
[80] M. Mollazadeh, M. Mohammadi-Khanaposhtani, A. Zonouzi, H. Nadri, Z. Najafi, B. Larijani, M. Mahdavi, New benzyl pyridinium derivatives bearing 2, 4-dioxo-chroman moiety as potent agents for treatment of Alzheimer's disease: Design, synthesis, biological evaluation, and docking study, Bioorg. Chem. 87 (2019) 506–515.